

2016

An effective method to reduce smearing in machining of metallic foams using ice as an infiltrant

Vishal Vijaykumar Mane
Iowa State University

Follow this and additional works at: <https://lib.dr.iastate.edu/etd>

 Part of the [Industrial Engineering Commons](#)

Recommended Citation

Mane, Vishal Vijaykumar, "An effective method to reduce smearing in machining of metallic foams using ice as an infiltrant" (2016). *Graduate Theses and Dissertations*. 15054.
<https://lib.dr.iastate.edu/etd/15054>

This Thesis is brought to you for free and open access by the Iowa State University Capstones, Theses and Dissertations at Iowa State University Digital Repository. It has been accepted for inclusion in Graduate Theses and Dissertations by an authorized administrator of Iowa State University Digital Repository. For more information, please contact digirep@iastate.edu.

**An effective method to reduce smearing in machining of metallic foams
using ice as an infiltrant**

by

Vishal Vijaykumar Mane

A thesis submitted to the graduate faculty
in partial fulfillment of the requirements for the degree of

MASTER OF SCIENCE

Major: Industrial Engineering

Program of Study Committee:
Matthew C. Frank, Major Professor
Frank E. Peters
James H. Oliver

Iowa State University

Ames, Iowa

2016

Copyright © Vishal Vijaykumar Mane, 2016. All rights reserved.

TABLE OF CONTENTS

	Page
LIST OF FIGURES	iv
LIST OF TABLES	vi
NOMENCLATURE	vii
ACKNOWLEDGMENTS	viii
ABSTRACT	ix
CHAPTER 1 INTRODUCTION	1
CHAPTER 2 LITERATURE REVIEW	7
CHAPTER 3 A METHOD TO REDUCE SMEARING IN THE MACHINING OF METALLIC FOAMS USING INFILTRATION	15
Abstract	15
3.1 Introduction	16
3.2 Related Work	19
3.3 Methodology	21
3.3.1 Infiltration Method	22
3.3.2 Machine Setup and Cutting Methodology	24
3.3.3 Surface Porosity Measurement & Method	26
3.3.4 Tool Wear Analysis	29
3.3.5 Design of Experiments	30
3.3.6 Analysis of Variance (ANOVA)	31
3.4 Results and Discussion	32
3.5 Implementation	38
3.6 Conclusion	42
CHAPTER 4 CONCLUSION AND FUTURE WORK	44
REFERENCES	46
APPENDIX A. 2 ³ FULL FACTORIAL EXPERIMENTAL RESULTS FOR WAX TRIALS	50

APPENDIX B. AVERAGE 2^3 FULL FACTORIAL SURFACE POROSITY	
RESULTS PER FACTOR FOR WAX TRIALS.....	52
APPENDIX C. 2^3 FULL FACTORIAL ANOVA ALL FACTOR ANALYSIS	
FOR WAX TRIALS – TOOL A.....	53
APPENDIX D. 2^3 FULL FACTORIAL ANOVA NORMAL PLOT OF	
EFFECTS FOR WAX TRIALS – TOOL A	54
APPENDIX E. 2^3 FULL FACTORIAL DESIGN OF EXPERIMENTS FOR ICE	
TRIALS	56
APPENDIX F. FITTED EFFECTS OF ICE TRIALS	57
APPENDIX G. 2^3 FULL FACTORIAL ANOVA ALL FACTOR ANALYSIS	
FOR ICE TRIALS	58
APPENDIX H. 2^3 FULL FACTORIAL ANOVA INDIVIDUAL FACTOR	
ANALYSIS FOR ICE TRIALS	59
APPENDIX I. PREDICTION PROFILER	61

LIST OF FIGURES

	Page
Figure 1.1 Aluminum foam	1
Figure 1.2 Comparison between open and closed cell foams	2
Figure 1.3 Trabecular Metal TM before and after machining	3
Figure 1.4 Comparison between infiltrated and non-infiltrated sample	4
Figure 2.1 Relative density comparison of metallic foams	8
Figure 2.2 Steps to manufacture metallic implants	9
Figure 2.3 Porosity comparison between cancellous bone and Trabecular Metal TM	10
Figure 2.4 FE-SEM micrographs illustrating the hFOB cell morphologies	11
Figure 2.5 Cutting mechanism interrupted by pores	13
Figure 2.6 Deformation zone during machining of porous metals	14
Figure 3.1 Porosity comparison between cancellous bone and Trabecular Metal TM	16
Figure 3.2 Cutting mechanism interrupted by pores	19
Figure 3.3 Deformation zone during machining of porous metals	19
Figure 3.4 Bending mechanism of porous cell walls	20
Figure 3.5 Resultant smeared surface after machining	21
Figure 3.6 Infiltration process and post machined sample	22
Figure 3.7 Steps in infiltration process	23
Figure 3.8 Machining setup	24
Figure 3.9 Machined samples	25
Figure 3.10 Porosity comparison between non-machined and machined sample	27
Figure 3.11 Locations of microscopic images on the machined surface	27

Figure 3.12 Reticle analysis method	28
Figure 3.13 Effect of infiltrant on surface smearing	32
Figure 3.14 Fitted main effect chart of tool A	36
Figure 3.15 One-way ANOVA for different combinations	38
Figure 3.16 CT scan data	39
Figure 3.17 CNC-RP method	40
Figure 3.18 CAD model and sample bone implant	41

LIST OF TABLES

	Page
Table 3.1 2 ³ full factorial experimental conditions	31
Table 3.2 Investigated Machining Parameters	33
Table 3.3 Confidence Interval Test	34
Table 3.4 t-test results	34
Table 3.5 All factorial results using Tool A (ANOVA)	35
Table 3.6 p-value results using Tool A	36
Table 3.7 Indicator Function Parameterization (ANOVA)	37
Table 3.8 Surface porosity analysis of TM bone fracture fragment	42

NOMENCLATURE

TM	Trabecular Metal
Ta	Tantalum
Ti	Titanium
W	Tungsten
RP	Rapid Prototyping
CNC	Computer Numerically Controlled
MAM	Metal based Additive Manufacturing
SLM	Selective Laser Melting
EBM	Electron Beam Melting
SLA	Stereolithography
SLS	Selective Laser Sintering
FDM	Fused Deposition Modeling
DMLS	Direct Metal Laser Sintering
in	Inches

ACKNOWLEDGMENTS

First and foremost, I must express my very profound gratitude to my parents, my father Shri. Vijaykumar Mane, and my mother Smt. Lata Mane for providing me with an opportunity to pursue my Master's degree at Iowa State University. Also, for providing me with unfailing support and continuous encouragement throughout my years of study and through the process of researching and writing this thesis. I would like to thank my sister, Miss Vaishali Mane for providing me moral support whenever I was going through tough times.

I would like to offer my sincerest gratitude to my advisor, Dr. Mathew Frank. The door to Dr. Frank's office was always open whenever I ran into a trouble spot or had a question about my research or writing. He consistently allowed this thesis to be my own work, but steered me in the right direction whenever he thought I needed it.

I would also like to thank my committee members, Dr. Frank Peters and Dr. James Oliver for their guidance and support throughout the course of this research. I would like to thank Dr. Anna Peterson for providing much needed guidance in statistical analysis in my research. Without their expertise and guidance, my research would not have been possible.

In addition, I would also like to thank Zaine Talley, Daniel Robinson and Ronald Harms for putting in the time to machine metallic foam samples. I would like to thank my friends, colleagues, the department faculty and staff for making my time at Iowa State University a wonderful experience.

Finally, I must thank my partner Miss Chaitali Chinoy for providing me with unfailing support. She was always there cheering me up and standing by me through the good times and bad. Thank you.

ABSTRACT

This thesis focuses on a new method to reduce surface smearing caused by machining metallic foams. Metallic foam is a cellular structure, similar to foam, but made of metal. This study demonstrates a new method which uses ice as an infiltrant, built upon previous work which used wax as an infiltrant. Ice as an infiltrant helps cell walls by providing them support. In this study, experiments were conducted on a metallic foam named Trabecular Metal™ (TM). It is made of elemental tantalum (Ta) which is one of the most chemically stable and biologically inert materials. This specific characteristic of Ta makes it suitable for orthopedic metal implants. Research tasks include replication of the results from previous methods (using wax as an infiltrant), and then proof of concept for ice as a suitable material for infiltrant. All machining trials on ice infiltrated TM were conducted in a cryogenic environment. It avoided melting of ice due to excessive heat produced because of machining process. The final task includes optimization of the significant process parameters to make it faster and efficient. Results indicated that the use of ice as an infiltrant worked as well as wax, while also reducing the possibility of having any detrimental residue left inside the implant. By analyzing statistics on collected data, it was also concluded that feed rate is the most significant factor to reduce the surface smearing of metallic foam, Spindle Speed and Corner Radius were also shown to have a significant effect. The impact of this research is that it will help to machine metallic foams more efficiently than before, now with an inert infiltrant material that is easy to remove after processing.

CHAPTER 1. INTRODUCTION

In addition to solid metals, another form of metals exists, called metallic foams (also known as cellular metal, porous metal, metal foam, and metal sponge) which are cellular structures consisting of metal. It is a newer class of engineering materials with low densities, novel physical and mechanical properties and exceptional thermal, electrical, and acoustic properties [1, 2]. Figure 1.1 shows an example of an aluminum metal foam.

As of today, commercially available metal foams are made from aluminum (Al), nickel (Ni), titanium (Ti), copper (Cu), tungsten (W) and tantalum (Ta) [1]. Several methods exist for the manufacturing of metallic foams from magnesium (Mg), lead (Pb), zinc (Zn), Cu, bronze, Ti, steel

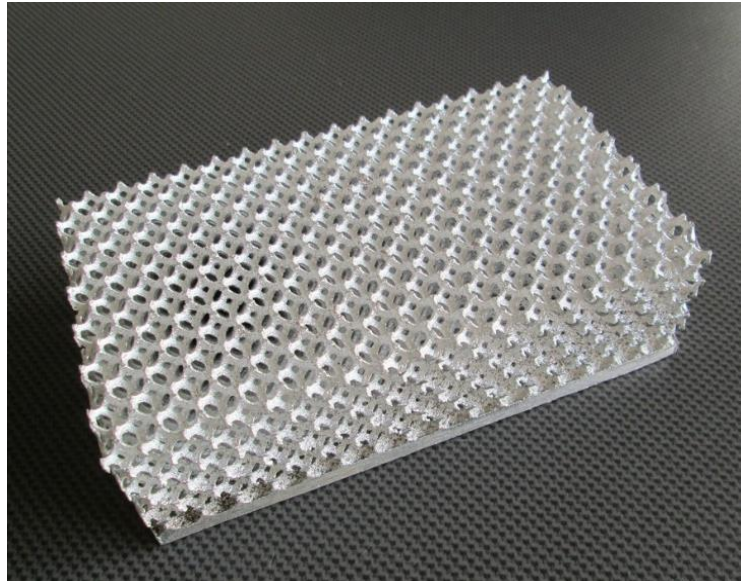


Figure 1.1 – *Aluminum foam* [45].

and gold (Au) [2]. Structurally, metallic foams are characterized by their cell topology (open cells or closed cells). As the name indicates, open cell metal foams contain open cell topology vs closed cell topology in closed cell metal foams. Open cell metallic foams have a wide variety of applications, from heat exchangers, energy absorption, manufacturing, aerospace, chemical and medical industries. On the other hand, closed cell metallic foams have their own set of applications, including construction, aerospace, and automotive industries.

Figure 1.2 illustrates the visual difference between the two types.

Primarily there are 9 different methods being used to make metal foams [2]. They are as follows, 1) Bubbling gas, 2) Stirring foaming agent, 3) Consolidation of metal powder, 4) Polymer foam precursor, 5) Vapor phase deposition or electrodeposition of metal, 6) Trapping of high-pressure inert gas in pores by powder hot isostatic pressing, 7) Sintering of hollow spheres, 8) Co-pressing of metal powder with a leachable powder, 9) Dissolution of gas [2]. For commercial production, only the first 5 methods are generally recommended.

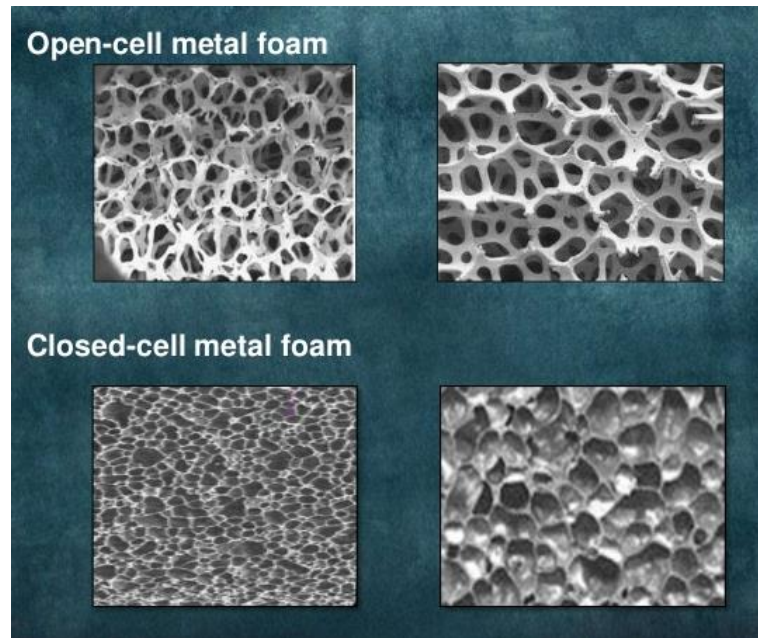


Figure 1.2 – Difference between open cell metal foam vs closed cell metal foam [44].

Due to favorable results related to biocompatibility and structural properties over the years, open cell metallic foams have become a preferred choice for the medical industry [1, 5]. In previous studies in the medical field, it has been shown that in closed-cell foams there is a thin membrane of metal present, whilst in open-cell foams the interconnected individual cells allow tissue to infiltrate the foam and anchor it into position [3]. The open cell structure

of metallic foams allows bone to grow into and over the metal through the process called Osseointegration. Porous structure also allows blood flow through the implant, ultimately promoting bone ingrowth into the implant.

For this thesis, Trabecular Metal™ composed of elemental Ta was chosen as the metallic foam. It is shown to have high fatigue strength and compressive modulus which allows it to bend before breaking making it an excellent fit for orthopedic implants [4]. TM structure supports bone integration, bone remodeling, and vascularization [5]. This property enhances new bone formation and formation of capillaries [6]. TM was designed for the sole purpose of imitating properties of natural bone. The consensus among several sources estimates the surface porosity for TM between 70 to 85% [10, 11, 12, 13, 14].

Surface porosity of the metallic foams decreases due to a smearing effect which occurs during machining of metallic foams in traditional machining methods [1, 2, 15, 16, 17, 18]. Since metallic foam has cellular structure, the interconnected cell wall offers little to no support against high machining forces observed in traditional machining [7]. Surface smearing occurs due to collapsing of the cell walls brought about by machining forces, which is also dependent on pore size and shape of individual cells. Figure 1.3 shows the smearing effect caused by machining of metal foam without any infiltrant [8].

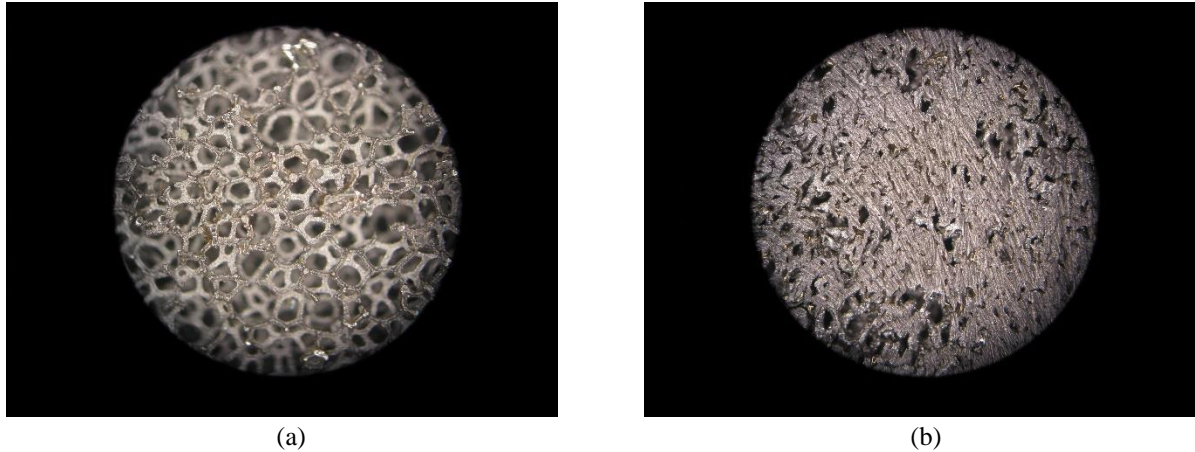


Figure 1.3 – *Trabecular Metal™ (a) before and (b) after machining [8].*

Traditionally, electric discharge machining (EDM), especially Wire EDM was the method of choice in the industry to machine metallic foams [7]. Wire EDM uses a small diameter (commonly down to 0.001 in dia.) wire. It uses a series of electrical discharges (sparks) that are produced between an accurately positioned moving wire (the electrode) and the workpiece. High frequency pulses of alternating or direct current are discharged from the wire to the workpiece with a very small spark gap through an insulated dielectric fluid (water or oil) [9]. In 2008 a method was developed to machine metallic foams without occurrence of smearing [2, 20]. This patent pending method was based on the principle of using wax as an infiltrant between pores of open cell metal foams. The infiltrated wax provides supports to cell walls against machining forces, ultimately resulting in better surface porosity of machined metallic foam [8]. Figure 1.4a shows wax infiltrated sample after machining and Figure 1.4b shows the same sample after wax is removed.

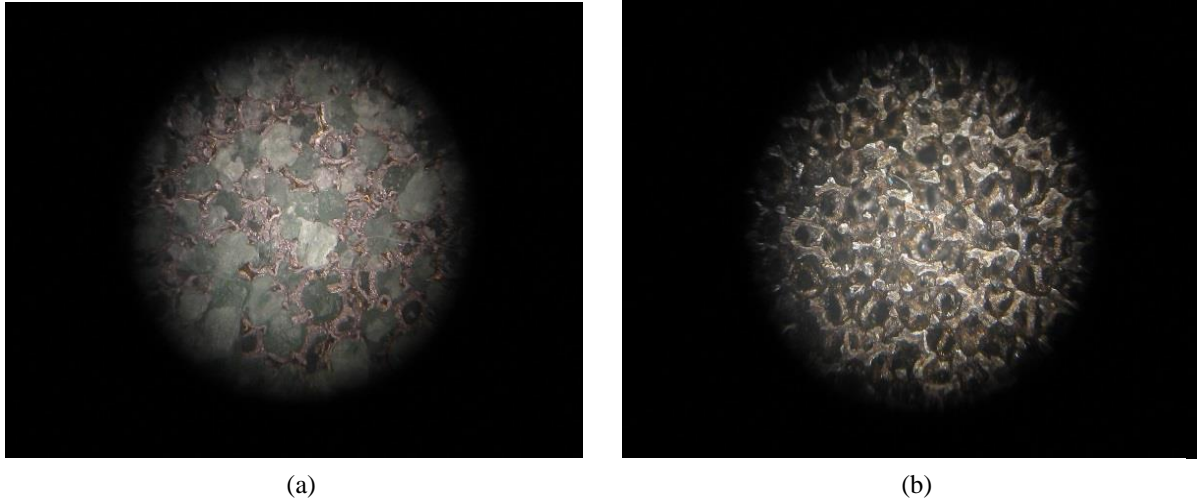


Figure 1.4 – (a) Wax infiltrated sample, (b) After wax was removed

The infiltrant method allowed for the successful machining of metallic foam implants without smearing; however, the work was limited to wax as an infiltrant. It was predicted that combining the infiltration method with rapid prototyping (RP) technology may make manufacturing of custom orthopedic implants feasible in the future [8]. The previous method using wax required, on average, 30 minutes of post processing time for each implant. Post processing included heating the sample to melt and wick out the wax present inside the pores of metallic foam. It was concluded that a better infiltrant might help to make the current process better.

This thesis focuses on a new method using ice as an infiltrant and the general optimization of the process. To achieve the main goal of developing this new method, it is further broken down into two sub-objectives. The first sub-objective is to replicate the results from using wax as an infiltrant and then successfully replace the wax with ice (since ice as an infiltrant has several advantages over wax). To achieve this, two major tasks needed to be completed; the first of which is verification of previous experimental results by conducting trials using the same machining parameters using wax as an infiltrant. The second task involves

conducting experiments using the wax settings, to prove whether ice will work as an infiltrant. The second sub-objective of the research is to optimize machining parameters for the process using ice, to make it faster and more efficient. This sub objective will likewise require two major tasks; task one being designing and conducting a set of experiments on ice infiltrant parameters. Then, task two involves analyzing results and determining optimized machining parameters to reduce the processing time of machining of metallic foams. It is predicted that using these investigated parameters in the proposed method, along with the combination of rapid machining, will allow one to machine metallic foam without having the surface smeared.

The remainder of this Thesis is organized as follows: Chapter 2 discusses relevant literature review, providing detailed background knowledge on the topics of this thesis. This is followed by the overall solution methodology in Chapter 3, while Chapter 4 provides statistical analysis and results. Finally, Chapter presents conclusions and proposed future work.

CHAPTER 2. LITERATURE REVIEW

A metallic foam is a class of materials with low density and novel physical, mechanical, thermal, electrical, and acoustic properties [2]. The term “metallic foam” is often used in a generic way to describe materials that are often not foam in a strict sense. They are also known as Cellular metals, Porous metals, Metal foams and Metal sponges [10]. Sea Coral found in nature can be considered a kind of foam, which can be used for various applications. Properties of metallic foam are mainly dependent on three factors; 1) material properties of the metal from which the foam is made, 2) relative density and 3) cell topology [2]. The material properties of the metal define the properties of metallic foam such as physical and mechanical properties. Relative density, ρ^*/ρ_s ; where ρ^* is defined as the density of the metallic foam and ρ_s , the density of the solid metal from which cell wall is made up of [11]. Relative density of cellular bone has been found to be approximately 0.20. To be considered as a genuine cellular material, the relative density value must be less than 0.30 [11]. Cell topology mainly decides potential applications of the foam and its classification (open cell or closed cell) [1, 22].

There are different methods available to manufacture metallic foams. Traditionally nine major methods have been utilized, including; 1) Bubbling gas, 2) Stirring foaming agent, 3) Consolidation of metal powder, 4) Polymer foam precursor, 5) Vapor phase deposition or electrodeposition of metal, 6) Trapping of high-pressure inert gas in pores by powder hot isostatic pressing, 7) Sintering of hollow spheres, 8) Co-pressing of metal powder with a leachable powder and 9) Dissolution of gas [2]. Of these, the first 5 methods are mainly used to produce metallic foam on commercial scale. Figure 2.1 summarizes cell size range and cell

type (open or closed) and relative densities that can be manufactured with current manufacturing processes.

Along with these traditional methods, the demand for implants with customized mechanical performance is increasing

[12]. Additive manufacturing

(AM) provides opportunities

to manufacture metallic

foams [23, 24]. It has been

proven that for obtaining optimal

internal structure for porous implants,

digital topology optimization is a

powerful tool [12]. AM has

been growing as a method in

the industry to manufacture porous metal

implant with high accuracy for external shape

along with internal architecture [24, 25]. Electron beam melting (EBM) and selective laser

melting (SLM) use layer based principles of fabrication methods [24, 26, 27]. EBM can only

be used for the manufacturing of conductive parts (metals), since it uses an electron beam as

a power source. On the other hand, SLM can manufacture metals as well as polymers and ceramic

as it uses a laser beam as a power source. In industrial manufacturing SLM is preferred

over EBM because SLM can produce minute details, it gives better surface roughness

conductive to implants and resolution needed for implants [24, 25].

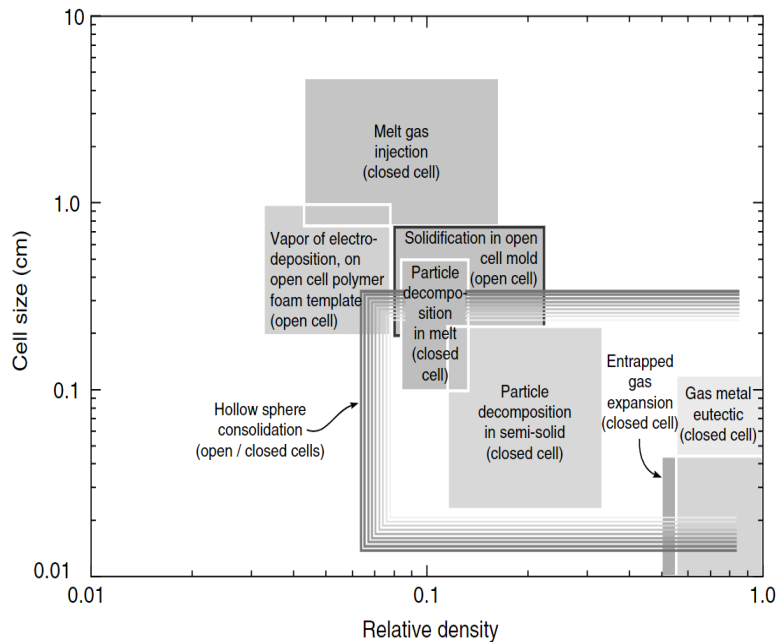


Figure 2.1 – Range of cell size and relative density for the different metal foam manufacturing method [2].

Figure 2.2 shows a schematic diagram of the entire process, which covers all the steps starting from design, additive manufacturing to final product.

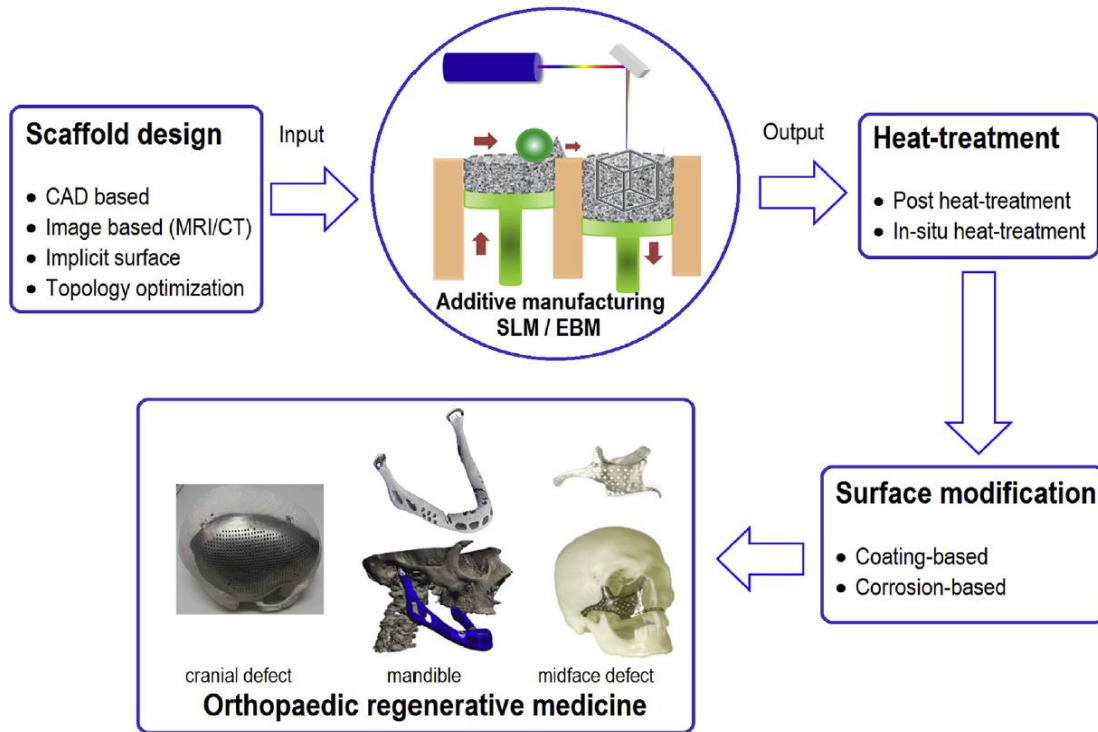


Figure 2.2 – Schematic diagram shows steps to manufacture metal implants with examples [24, 25].

Different industries use metallic foams for different processes. Metallic foam can be a solution for a problem, depending on conditions, which are summarized below according to the keywords used in the industry [10]. Morphology is used to decide type, amount and scale of porosity needed. Metallurgy determines the metal or alloy needed to manufacture the foam. Processing determines the different ways with which one can manufacture metallic foam. One can use a combination of different methods to manufacture the foam as well. Economic analysis determines the cost associated with manufacturing, along with volume [10]. Applications of metallic foams range from automotive to medical industries. The automotive

industry uses metallic foam for lightweight construction, crash energy absorption and damping insulation for noise control [1, 4, 21]. The aerospace industry uses metallic foams to replace expensive honeycomb structures with metallic foamed sheets or sandwich panel structures [10]. The use of metallic foams helps to reduce cost associated with structures and provides a high performance output. Uses in the medical industry includes Ti foam dental implants while Mg foam implants are best suited for bio-degradable implants that will be gradually absorbed by the body over time through convalescence [10].

Open cell metallic foam called Trabecular Metal foam (TM), made from tantalum, is used for this thesis. It is produced through pyrolysis of a thermosetting polymer foam creating a low density vitreous carbon skeleton [13]. Since it is very important to maintain metal density and structural porosity, TM is manufactured through a process called vapor deposition onto the carbon skeleton [15, 29, 30]. Before final layer of vapor deposition, metal is cut to a desired shape to maintain dimensional accuracy. The carbon skeleton is burned off during the process of vapor deposition, leaving a purely tantalum metallic foam structure [7]. TM has similar structure as cancellous bone which makes it suitable material for medical implants. Figure 2.3 provides a comparison between porous cellular bone and porous TM.

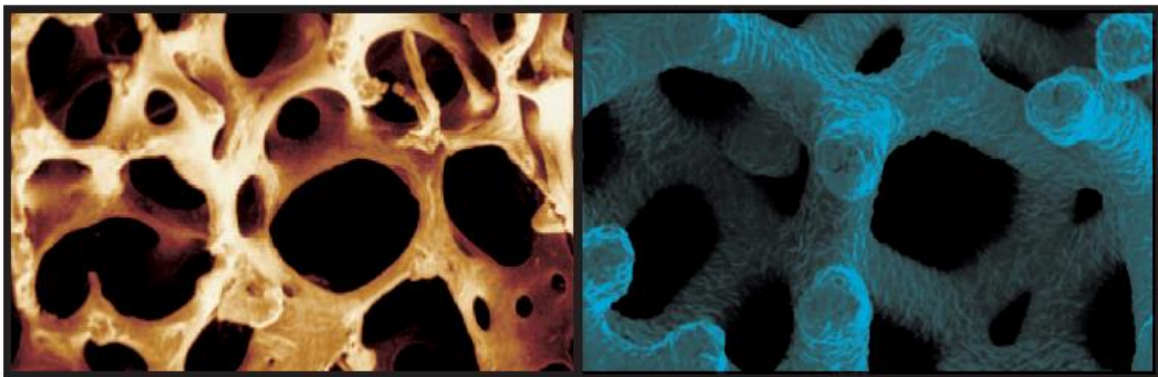


Figure 2.3 – Porous cancellous bone (Left) with porous Trabecular Metal™ (Right) [43].

Ti is one of the most chemically stable and biologically inert metals used in orthopedic implants, making it highly biocompatible and corrosion-resistant [4]. Biocompatibility is generally defined as the ability of a biomaterial to perform its desired function without undesirable effects [14]. Ti has a high coefficient of friction, which makes it an ideal material for an excellent scratch fit [15]. Its ability to resist corrosion along with possession of high strength makes Ti a suitable material for orthopedic implants [4]. Figure 2.4 shows cell morphology on Ti and Ta samples over different periods of time. It has been found that Ta has 6 times more favorable results over Ti with respect to bone growth.

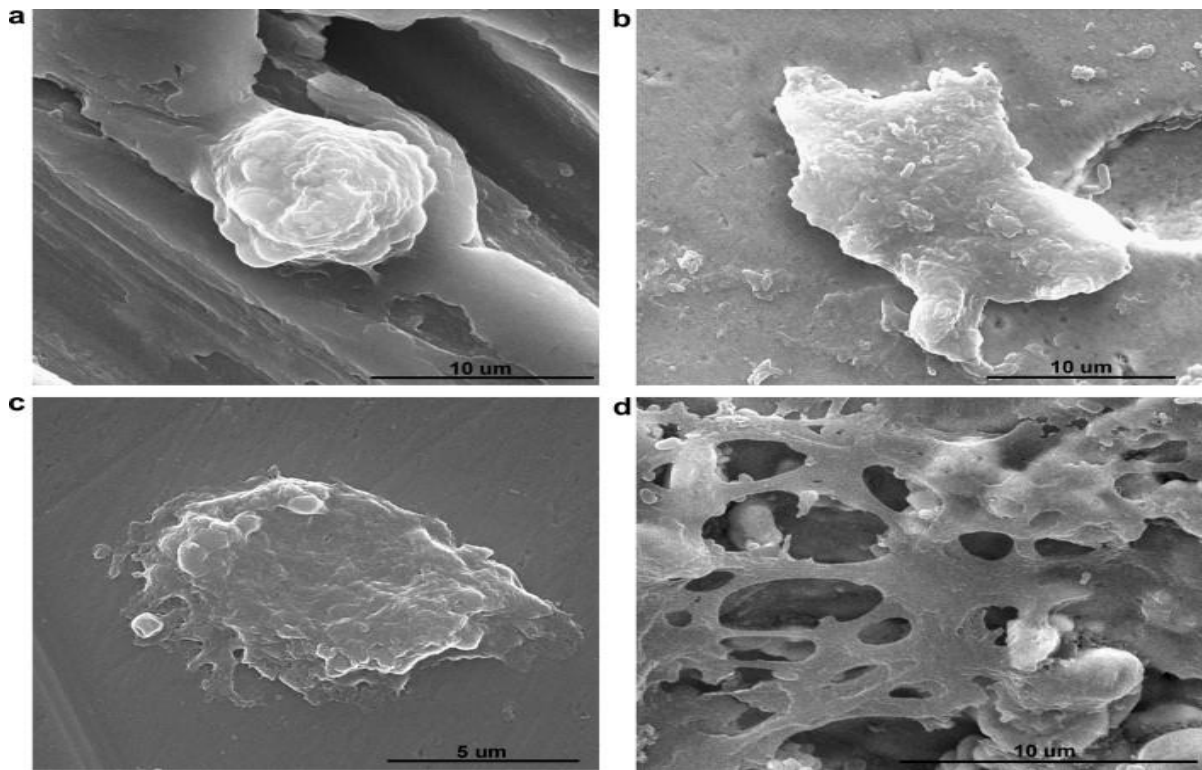


Figure 2.4 – FE-SEM micrographs illustrating the hFOB cell morphologies. (a) Ti surface after 3 days. (b) Ta surface after 3 days. (c) Ti surface after 14 days. (d) Ta surface after 14 days [13].

Computed Tomography (CT) is mainly used to observe internal structures of the human body. CT scan data has been used to produce additively manufactured parts using CAD models generated using scan data [33, 34, 35].

A method was outlined to design and manufacture an orthopedic implant, especially for the femur [16]. This method used CT data to machine the medical implants instead of printing them using AM. To machine medical implants using CNC machining, toolpaths are required and scan data was used to create the 3D model, from which toolpaths were created [16]. This process can serve only certain geometric implants because of requirement of special fixture and cutting angles [16]. Another study was conducted on a similar idea of using CT data for manufacturing medical implants via machining. It was concluded that rapid prototype models could be made available in 24 hours after approval of CT images from the surgeon [17]. However, overall product development time required turned out to be 8 days, mainly due to chipping that occurred during machining of Ti [17].

It has been shown that the use of conventional machining processes to machine low-density metallic foam can cause severe surface distortion and smearing [2]. Some non-conventional machining and cutting processes like EDM, wire EDM, high-speed fly cutting, and water-jet cutting was shown to give final products with less distortion and smearing [2]. In particular, it has been found that conventional machining of TM (using a lathe) resulted in surface pore occlusion [7]. This study was conducted to study the resulting surface characteristics of TM using conventional machining processes. A study was conducted on porous Ti to investigate surface smearing effects caused by face milling and peripheral grinding. To study the effects of milling in detail, both up-milling (conventional) and down-milling were performed [18].

Results concluded that milling performed on samples using cemented carbide inserts had better surface porosity. Also, samples machined with high cutting speed, low depth of cut and low feed per tooth showed better results [18]. It was also shown that silicon carbide grinding wheels produced better results as compared to corundum grinding wheels [18]. Another study was conducted to evaluate the combined effects of tool geometry, tool material properties, work material properties, and machining conditions on porous tungsten [19]. Initial observations of this study supported the hypothesis that, geometry of cutting tool and radius of cutting edge are significant factors influencing surface smearing of porous tungsten [19]. A recent study provided a correlation of cutting forces and surface porosity of porous Ti metallic foam manufactured using powder metallurgy (PM). It was concluded that structural porosity of Ti foam has a significant effect on cutting forces [20]. However further detailed experimentation is required to study the correlation in detail. Figure 2.5 shows the cutting mechanism on a porous sample

which is being interrupted by pores present in the metallic foam. This mechanism further leads to another cutting phenomenon known as deformation. Deformation theory demonstrates the formation of a de-

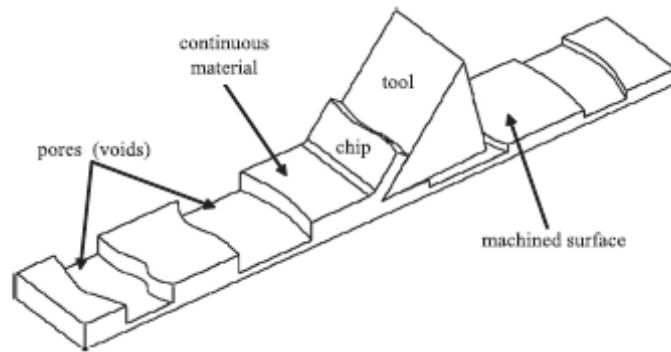


Figure 2.5 – Cutting mechanism interrupted by pores [20].

formed layer during machining [21]. Theory also suggests that lower cutting forces results in better surface porosity on metallic foams and longer tool-life [21]. The use of cryogenic machining for porous tungsten was shown to eliminate the necessity of plastic infiltrant along with a reduction in smearing [22].

Figure 2.6 illustrates the deformation mechanism during machining of metallic foams as dis-

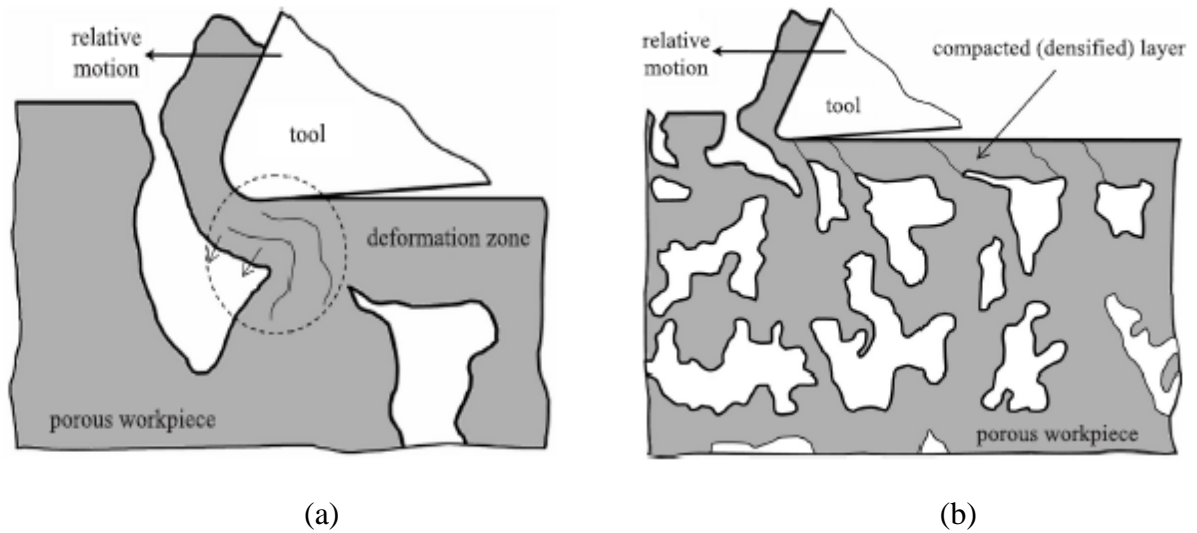


Figure 2.6 – Deformation zone (a) and dense layer formation because of machining [21].

cussed above. It was also concluded that low cutting radii of cutting tool ($r_{\beta} \approx 2 \mu\text{m}$) resulted in optimum surface quality [22].

The following chapter introduces a new method to avoid smearing, through the use of an infiltrant material to support metal foam pores. It further describes an additional infiltrant material beyond previous work, namely, ice.

CHAPTER 3.**A METHOD TO REDUCE SMEARING IN THE MACHINING OF METALLIC
FOAMS USING INFILTRATION****Vishal V. Mane, Christopher V. Hunt, Matthew C. Frank**

Department of Industrial and Manufacturing Systems Engineering, Iowa State University, Ames, Iowa 50011

A Journal Paper to be submitted; containing excerpts from Hunt, 2009

Abstract: This paper proposes a new method to reduce surface smearing in the machining of metallic foam through the use of an infiltrant. Metallic foams have been used in various industries from construction, building, aerospace, automotive to biomedical implants. The porosity of the foam is critical, for example, bone implants rely on this porosity for proper bone growth onto/into the implant. Traditionally, Electrical Discharge Machining (EDM) is the most preferred method to machine metallic foams, but it has limitations. For example, wire EDM technology can be limited in the machining of complex geometric shapes because of restriction in available access to the surfaces. Traditional machining causes surface smearing that diminishes or destroys the surface porosity of the foam. This work proposes the use of an infiltrant before machining, where wax or ice serves to prevent cell walls from bending during machining, resulting in better surface porosity. Experiments were performed using cryogenic machining to prevent softening of the infiltrant from the heat of machining. Results indicate that machining feed rate was the most significant factor affecting surface porosity, followed by cutting speed, tool radius and infiltrant hardness.

3.1 Introduction: Metallic foams are a class of material with unique physical, thermal, electrical, and acoustic properties [2]. These properties of metallic foams render them suitable as a new class of materials for a wide range of industrial applications. One specific and important characteristic i.e. Open cell structure of metal foams allows them to be an excellent candidate for use in orthopedic implants. When implanted into the body the interconnected porous network allows for the flow of blood through the implant, which enables bone growth into the foam. This bone growth secures the implant attachment with the host bone through Osseointegration. Metallic foams frequently used in orthopedic implants come in forms of various alloys of titanium (Ti) and cobalt (Co), most commonly as Ti-6Al-4V and Co-Cr, respectively [44, 45, 46]. Other biocompatible materials that have been used in implants in the past include porous hydroxyapatite, coral, and natural allograft or autograft bone [23]. Material selection for orthopedic use depends on the implant type and the material's similarity to the physical and mechanical properties of the host bone. For this study, the type of metallic foam was chosen to be Trabecular Metal™ (TM), composed of elemental Tantalum (Ta). A research and development firm named Ultramet, developed and patented a method to manufacture porous Ta in early 1990s [29, 30]. Figure 3.1 illustrates the porosity comparison of cancellous bone with TM. It has high fatigue strength and a high compressive modulus which allows it to bend before breaking, making it excellent for orthopedic implants [4]. High porosity of TM enhances bone ingrowth along with extensive tis-

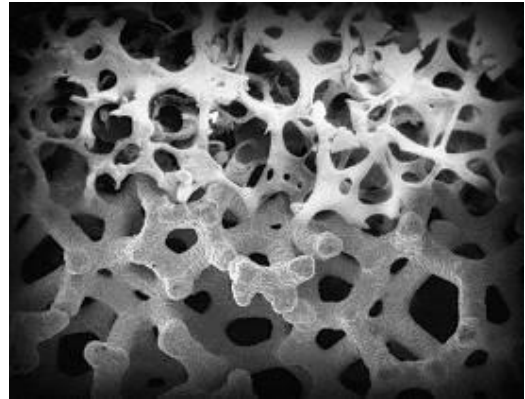


Figure 3.1 – Porosity comparison of cancellous bone (top) to TM (bottom) [43].

sue infiltration [10, 15]. TM structure supports bone integration, bone remodeling, and vascularization [5]. This enhances new bone formation and formation of capillaries [6]. TM was designed for the sole purpose of imitating properties of natural bone. Surface porosity value for TM ranges between 70 to 85% [10, 11, 12, 13, 14]. The crystalline micro texture of the tantalum struts that compose TM is conducive to direct bone apposition [15].

Electric discharge machining (EDM), especially Wire EDM, is the prominent method being used to machine metallic foams [7]. In the medical industry, it is very important to preserve porosity of metallic foam implants. Traditional machining causes a smeared surface on medical implants, which results in very low bone ingrowth [7]. Wire EDM uses a small diameter (usually 0.001 in) wire as a non-contact machining method which uses a series of electrical discharges (sparks) that are produced between an accurately positioned moving wire (the electrode) and the workpiece [9]. Limitations in machining complex geometric parts using EDM and Wire EDM processes provided the need to come up with a new method. This patent pending method is based on the principle of using an infiltrant in between pores. Infiltration methods provide a solution for the problem of smearing caused by machining [2, 20]. Infiltrated wax provides support to cell walls against machining forces ultimately resulting in better surface porosity of machined metallic foam [8]. Machining of metallic foam has several advantages over EDM and other processes. Machining helps to save cost of processing of metallic foam by reducing manufacturing steps [7]. The work presented in this study describes an initial step toward the custom manufacture of patient-specific orthopedic implants from a variety of biocompatible materials, including TM. Not only does this work apply to the standard orthopedic implants manufactured in generic sizes but more

importantly those one of a kind, custom bone implants needed to replace bone fracture fragments, bone tumor resections, or other segmental bone defects.

A novel method for machining metal foam is the subject of the research presented in this thesis. This method allows metal foams to be machined using computer numerically controlled (CNC) machining technology without the resultant surface smearing common with current practices. The ability to machine foam in a CNC machining center significantly increases the possibilities of geometric shapes that can be created. This patent-pending process involves infiltrating the stock foam material prior to machining in order to reduce the effect of surface smear left by the cutting process. Upon completion of all necessary machining steps, the infiltrant is removed from the machined part. It is predicted that surface smearing can be reduced by machining with the infiltrant. Utilizing this new process should not only reduce surface smearing but could inhibit machining debris from entering the porous structure during machining.

Through the use of this new infiltration process, CNC machining, and Rapid Prototyping (RP) technology, it may be possible to machine freeform geometric shapes from metal foam while minimizing the effect of surface smearing. The ultimate goal of this research is to determine the optimal machining parameters for milling Trabecular Metal™ in order to maintain a surface porosity value sufficient for successful Osseointegration in orthopedic surgery. The concept of customizable bone implants begins with the ability to machine custom geometries based on the patient's bone structure. However, the implant must also maintain a sufficient surface porosity to enable Osseointegration. The process described here is the first step in making these customizable, patient-specific bone implants become a reality.

3.2 Related Work: A recent study provided a correlation of cutting forces and surface porosity of porous Ti metallic foam manufactured using powder metallurgy (PM). It was concluded that structural porosity of Ti foam has a significant effect on cutting forces [20]. However further detailed experimentation is required to study the correlation in detail. Figure 3.2

shows the cutting mechanism on a porous sample which is being interrupted by pores present in the metallic foam. This mechanism further leads to another cutting phenomenon known as deformation. Defor-

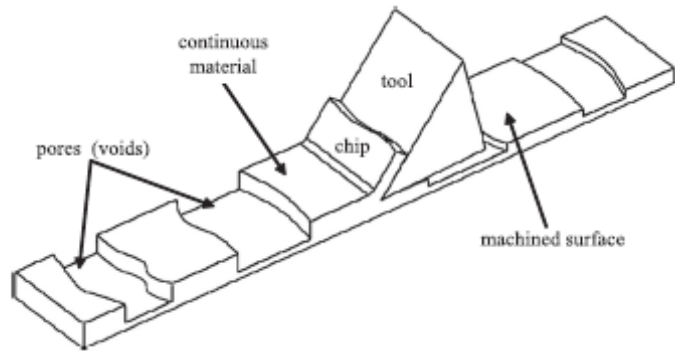


Figure 3.2 – Cutting mechanism interrupted by pores [20].

mation theory demonstrates the formation of a deformed layer during machining [21]. The theory also suggests that lower cutting forces results in better surface porosity on metallic foams and longer tool-life [21]. The use of cryogenic machining for porous tungsten was shown to eliminate the necessity of plastic infiltrant along with a reduction in smearing [22]. Figure 3.3 illustrates the deformation mechanism during machining of metallic foams as discussed

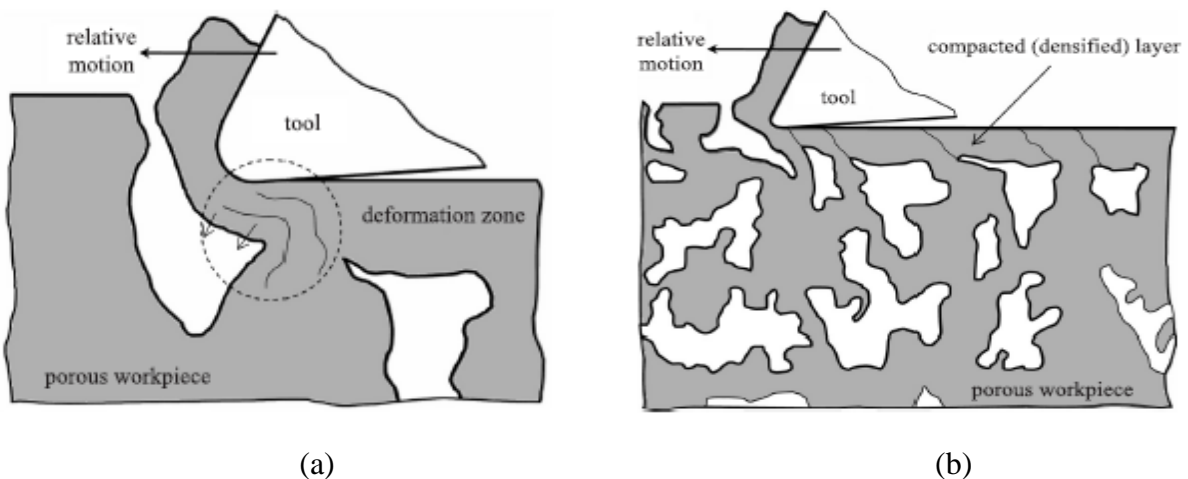


Figure 3.3 – Deformation zone (a) and dense layer formation because of machining [21].

above. It was also concluded that low cutting radii of cutting tool ($r_{\beta} \approx 2 \mu\text{m}$) resulted in optimum surface quality [22].

A study was conducted on porous Ti to investigate surface smearing effects caused by face milling and peripheral grinding. To study the effects of milling in detail, both up milling (conventional) and down milling were performed [18]. Results concluded that milling performed on the samples using cemented carbide inserts had better surface porosity. Also, the samples machined with high cutting speed, low depth of cut and low feed per tooth showed better results [18]. It has been found that silicon carbide grinding wheels ended up producing better results as compared to corundum grinding wheels [18]. Another study was conducted to see combined effects of tool geometry, tool material properties, work material properties, and machining conditions on the porous tungsten [19]. Initial observations of this study supported that the geometry of cutting tool and radius of cutting edge are the significant factors influencing surface smearing of porous tungsten [19]. This study provided base knowledge that can be used to produce analytical model which can predict surface smearing.

In Figure 3.4, the machining force created by the tool is represented by the load, P and travels in the same direction as the tool path. In order to maintain equilibrium, there is a resultant shear force and moment about the cantilevered end; these are represented by V_R and M_R , respectively [47, 48]. When the machining force is greater than the opposing shear force and moment, the strut (or beam) begins to bend; this bending motion creates a stress upon the struts of tantalum material.

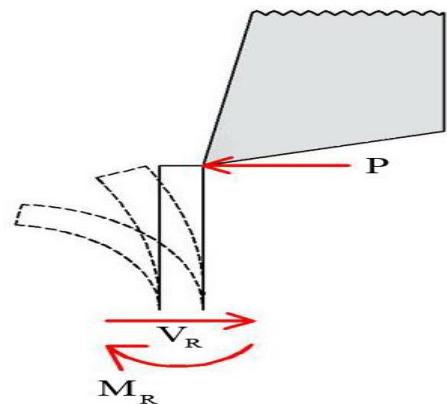


Figure 3.4 – The bending of a pore walls approximated by the bending of a cantilevered beam

When this stress exceeds the material yield strength, plastic deformation occurs and results in permanent pore occlusion. Owing to the temperature of the machining environment while being cut, the struts experience ductile fracture when they fail. This is due to the body centered cubic crystal structure of pure tantalum [24]. Cooling agent, liquid nitrogen is capable of reaching temperatures as low as -196°C . It was initially thought that while machining with the use of this coolant, the pure tantalum material would reach its ductile brittle transition temperature of -195°C causing the struts to experience brittle fracture when cut [25]. However, it was determined that the tantalum would never reach its transition temperature point due to conduction. Within the machine, the 0.5-inch diameter sample was held in a steel collet with a combined mass of approximately 0.91 kg. Due to this massive machining fixture, the small amount of tantalum being cut does not reach its transition temperature of -195°C . The cooling process is discussed in more detail later on in methodology section.

3.3 Methodology:

When the rotating tool moves across the cellular surface, the struts collapse, or bend over, closing the open voids. This smearing effect is shown as the tool cuts the porous material in Figure 3.5

At a microscopic level, this phenomenon looks much like a cantilevered beam experiencing a load upon its unsupported end (Figure 3.4). It is proposed that the infiltration method described in

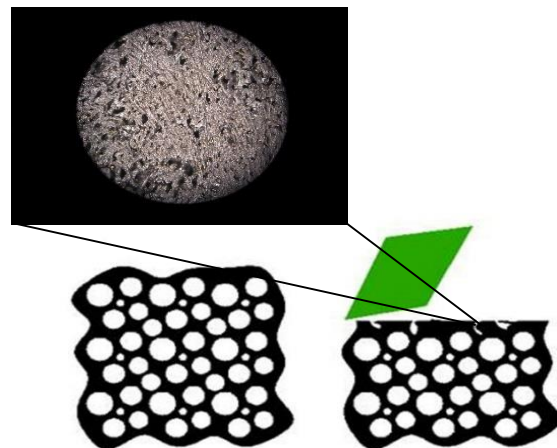


Figure 3.5 – Resultant smeared surface after traditional machining (Magnification 25X) [42].

this research could reduce the smearing effect. Infiltrant between pores of the foam will act as a structural member, stiffening the framework of the metal foam while still being cut by the tool. It is also suggested that the presence of infiltrate acts as a resistance against the cutting forces as a “backing” to the cell walls, resulting in prevention of the walls from bending. Infiltrant also prevents entry of foreign materials/contaminants into the metallic foam during machining. When the tool cuts through the infiltrated foam, the cellular struts are therefore braced by the infiltrant opposing the cutting forces and they remain or return to their upright position after being cut. For this study, two different kinds of infiltrant materials were used; machinable wax and ice. After machining, the infiltrant material was removed by simply melting (for ice) and melting and wicking (for wax). All trials were conducted on the metallic foam, Trabecular Metal (TM), as discussed in the introduction of this paper. All trials were performed in a 3-axis CNC machining center, using TM rods held in a stainless steel collet fixture.

3.3.1 Infiltration

Method: As a first infiltrant, two different commercially available waxes were used for this study. The hardness value for the waxes ranges from 50D to 52D [2, 20].

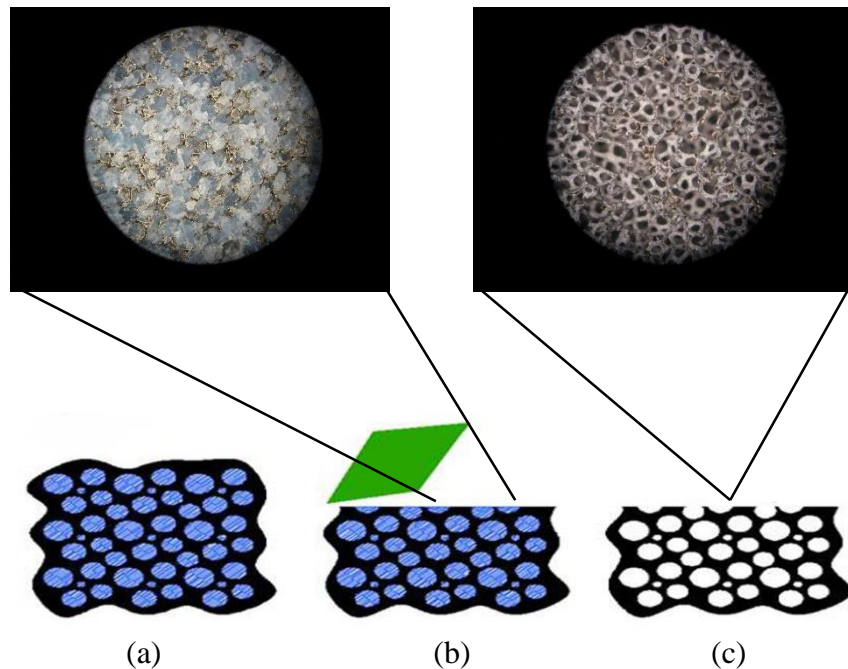


Figure 3.6 – (a) foam with an infiltrant, (b) infiltrated foam during machining, and (c) resulting porous surface after infiltrant is removed

Figure 3.6 shows infiltration process along with machined samples. The wax infiltration process began with melting the wax in a metal container upon a hot plate. A sample of TM was then placed in this container of wax so that one end (an approximate 0.75-inch-long section) was submerged in molten wax, Figure 3.7a. The container and sample were then removed from the hot plate and placed in a vacuum at 25 in. Hg for approximately 5 minutes. This removed all residual air bubbles from the molten wax and ensured that the TM sample was completely infiltrated. When all of the air had been evacuated from the molten wax and sample, the container and sample were removed from the vacuum environment and left at room temperature to solidify, Figure 3.7b. Once hardened, the sample was removed from the wax and any excess was removed, Figure 3.7c.

The ice infiltration process began with pouring purified water into a metal container designed to hold a sample, TM sample placed into the container, and the sample was placed in a vacuum as before. The container was then placed in a freezer for at least 6 hours and maintained frozen throughout the experiment. A sample ice-infiltrated TM rod is shown in Figure 3.7d.

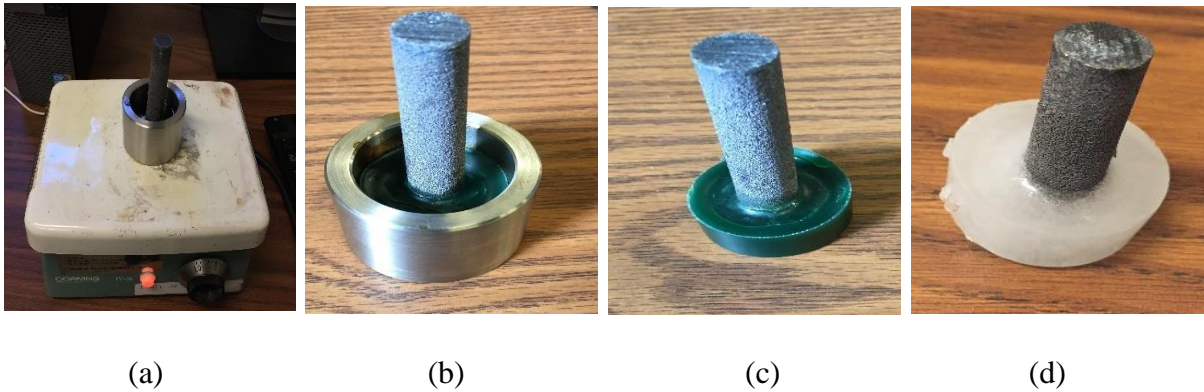


Figure 3.7 – Steps in Infiltration process

3.3.2 Machine Setup and Cutting Methodology: Conventional milling (Up Milling) was performed across the width of the sample, Figure 3.8.

The tool used for machining of wax samples was a 4 flute, High Speed Steel (HSS), non-coated, 0.5-inch diameter flat end mill. For ice samples, two different tools were used; 1) the same as for wax, and 2) the same tool with a corner radius of 0.002-in. Depth of cut was maintained at 0.02 in and width of cut at 0.25 in throughout all the trials.

For wax-infiltrated samples, two different feed rates of 10 and 40 in per minute were used and spindle speed

was maintained at 1000 revolutions per minute (rpm). For ice-infiltrated samples, feed rates were maintained at same levels as wax-infiltrated samples two different speeds of 1000 and 1200 rpm were used.



Figure 3.8 – Machining setup, coolant position along with ice infiltrated sample

Figure 3.9 illustrates a machined sample and its microscopic image taken at magnification of 12X.

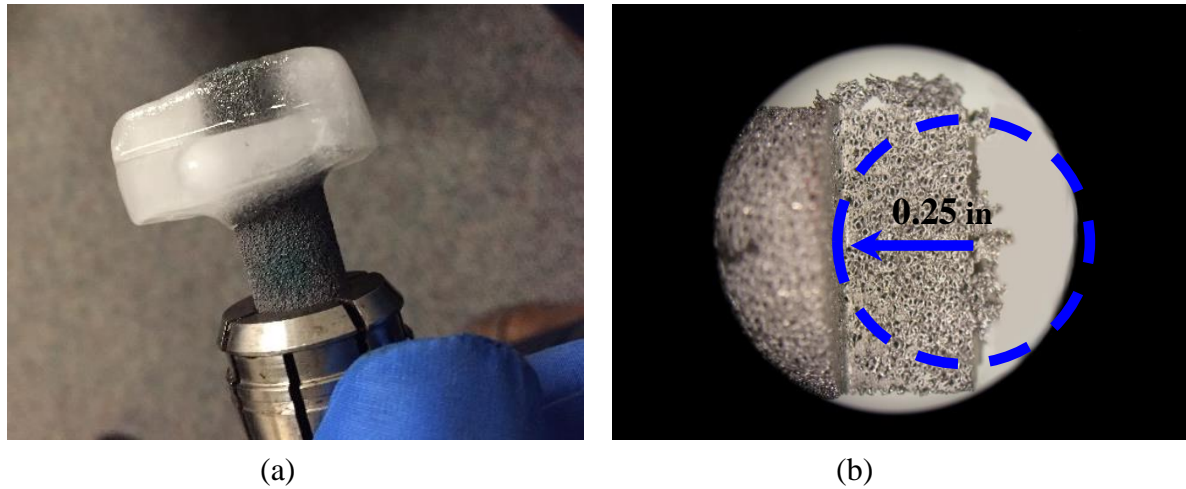


Figure 3.9 – (a) Ice- infiltrated sample after machining, (b) tool cutting position (Magnification 12X)

To give an idea of how much foam material this is removing as each flute cuts through, it was found that the strut thickness for TM at an average porosity of 77.5% (average of nominal range) is approximately 0.005 in [5]. This strut thickness is twice the feed value ran at 10 IPM and half that ran at 40 IPM. For wax trials, the two waxes used for the infiltration process will be referred to as “hard” and “very hard,” with hardness ratings of 50D and 52D, respectively. The hard wax begins to soften around 105°C (222°F) while the very hard wax will begin to melt at approximately 117°C (244°F). Preliminary machining experiments involved using Paraplast™ tissue embedding medium. This paraffin wax offered a significantly lower softening temperature and hardness rating.

Three machining temperatures were investigated while milling Trabecular Metal™, these included 21°C (room temperature, 69°F), -51°C (-59°F), and -196°C (-320°F). Technically, the trials ran at -196°C are considered to be in a cryogenic machining environment.

The two colder temperatures were reached using Cyto-Freeze™ spray (-51°C) and liquid nitrogen (-196°C) applied with a Brymill CRY-AC® cryosurgical device. Each sample was sprayed continuously for 30 seconds prior to starting the milling machine. After 30 seconds, the machine was started and the sample was continuously sprayed while the tool approached and cut through the material. While machining ice-infiltrated samples, only liquid nitrogen was used. It is critical to maintain the temperature of the sample since ice melts much faster (0°C or 32°F) as compared to wax; however, it was simple to remove the water after machining was finished. Wax infiltration method required much more rigorous post processing if the wax residue would need complete removal.

3.3.3 Surface Porosity Measurement and Method:

Image Capturing Procedure: After machining, each sample was removed from the 3-jaw chuck, post processed and observed under an optical microscope. The microscope used for this study was an Olympus™ SZX12, with lens 1X PF, zoom 25X, aperture fully opened. A computer triggered digital camera was used to capture images through the microscope using a Canon™ Power Shot S5 IS and an Alexis™ Scientific Digital Camera Microscope Adaptor. The camera settings used to capture all the images were, ISO-80, Shutter Speed-1/60 s,

F-4.0, Flash-OFF, T-2.0x, size- L. Image 3.10 below shows images of uncut TM and a machined TM sample that was ice-infiltrated.

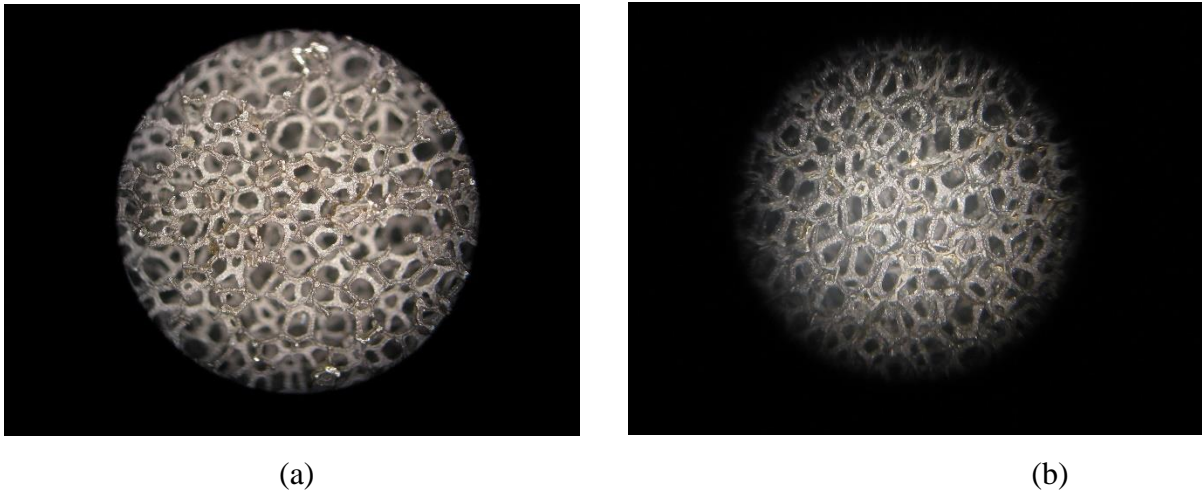


Figure 3.10 – (a) Fresh uncut TM sample, (b) Machined sample (Ice- infiltrated) (Magnification 25X)

To improve quality of the statistical analysis, 3 different images were taken for each cut. Images were taken at different locations about the surface of every cut, these locations were evenly spaced across the surface to ensure a comprehensive capture of data and are illustrated in Figure 3.11.

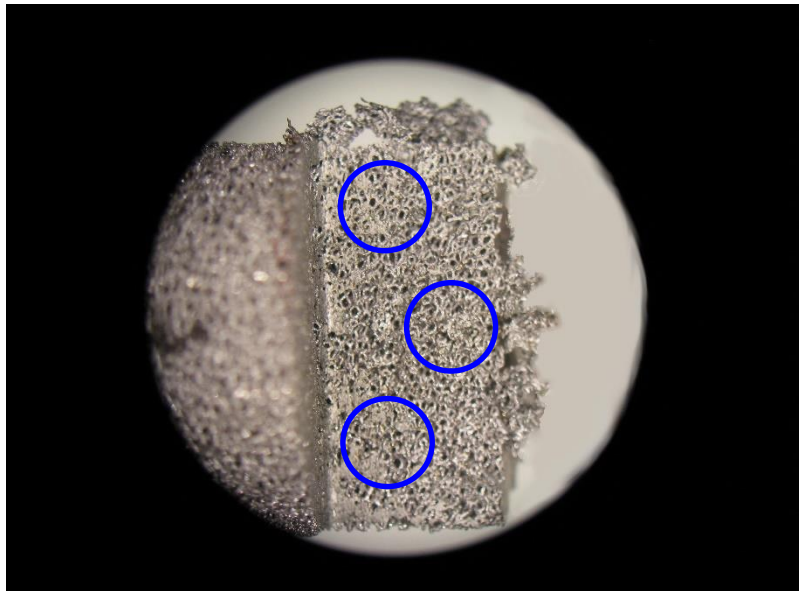


Figure 3.11 – Locations of microscopic images on the cut surface (Magnification of 12X)

Image Analysis Method: In order to evaluate porosity on the images, Attempts were made to measure surface porosity using software (ImageJ). Due to unfavorable and inaccurate results using software, a reticle grid analysis method was used to measure the samples. Each image was processed in Adobe™ Photoshop, where ten vertical and ten horizontal guide lines were imposed atop the image at equal spacing to create a grid. Since the all the captured images had a same size of 3264 X 2448 (pixels), the grid was created horizontally and vertically as per dimensions shown in Figure 3.12.

Each intersection which appears on metal (cut or uncut) at the surface layer of the foam was given a value of 1 and all other intersections counted as 0 (even if they appear over metal which is below the surface layer of metallic foam). The intersections of the guide lines made up 100 data points to be analyzed. Inter-

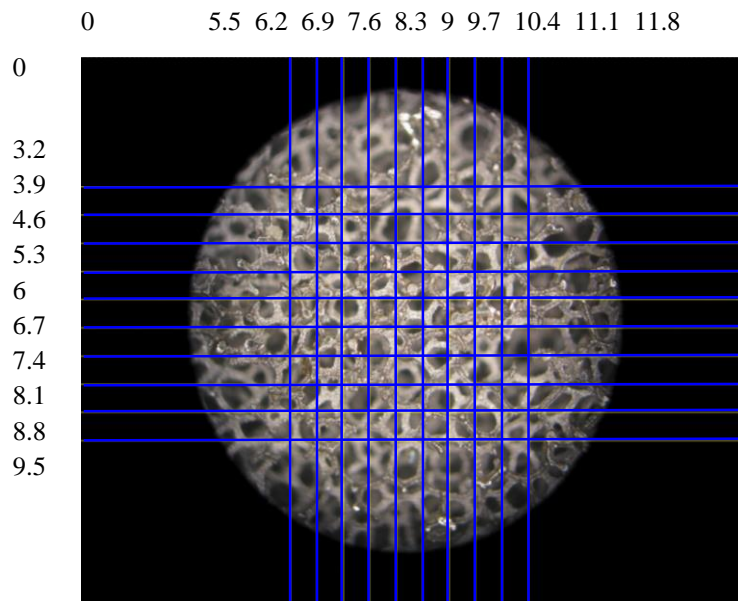


Figure 3.12 – Reticle grid imposed uncut TM sample

sections above open voids were counted and recorded. After all, 100 points had been analyzed, a ratio was calculated to determine surface porosity as a percentage of void space.

$$\text{Surface Porosity} = \frac{\# \text{ of intersections above void space}}{100}$$

For every cut, three images were taken, fit with a reticle, and surface porosity measurement recorded. The average of these three measurements was documented as the final surface porosity score for that specific cut.

The reticle analysis quantifies the amount of surface smearing that has occurred in the form of a measurement of surface porosity. A greater presence of pore occlusion corresponds to a lower surface porosity measurement, as this is a ratio of pore space to metal. Unprocessed TM has a nominal surface porosity of approximately 70 – 85% [10, 12, 14]. If a machining process does not induce surface smearing, the surface porosity of a cut sample should also be between 70 and 85%.

3.3.4 Tool Wear Analysis: Previous research endeavors have found that tool wear and cutting edge geometry variation can influence surface smearing during machining [38, 51]. An objective of this work was to determine how tool wear would influence the surface porosity of TM during machining. In order to evaluate this effect on surface smearing, the 2^3 full factorial machining experiment was performed with two different tools. Two previously unused tools were subject to a number of cuts in order to create different amounts of tool wear for each end mill. Over the course of 211 cuts, one tool sustained approximately 1.83 minutes (55 cuts) of cutting while the other endured approximately 5.32 minutes (156 cuts). Because these two tools were exactly alike, the collected data provided an indication of how a tool would affect surface porosity throughout its life.

The 2^3 full factorial experiment was first conducted with a “new” tool after approximately 1.39 minutes of cutting experience. Then a second experiment was performed using a “worn” tool that had incurred approximately 4.95 minutes of cutting time. For clarity in this

thesis, the new tool will be referred to as Tool A and the worn tool, Tool B. This allowed for a comprehensive comparison of how the three factors would influence surface porosity between using a relatively new tool and one that had experienced significant tool wear. The benefit of this analysis is that it provided an indication of when in a tool's life certain factors would have a significant effect on surface porosity, if any.

3.3.5 Design of Experiments: A 2^3 factorial design of experiment was used for this study.

The first design consisted of three different machining parameters, or factors, (infiltrant hardness, temperature, and feed rate) at two different levels (low and high). The second design consisted of three different machining parameters, (feed rate, spindle speed, and tool corner radius) at two different levels (low and high). Low and High values for the levels were chosen based on preliminary trials conducted in the lab and literature review. The benefit of using a 2^3 full factorial design is that it allows for several factors to be evaluated in a feasible number of experiments [26]. These factor values were chosen after a significant amount of evaluation through preliminary machining experiments. The trials shown in Table 3.1 and 3.2 were first randomized to ensure the elimination of any non-experimental variables or ambient conditions impacting the response [26]. Successive experiments were then designed based on the knowledge gained to make certain only the most relevant machining parameters and their settings were investigated. It was determined that upper and lower control limits for all collected data would be calculated at two standard deviations above and below the grand mean of a data set [27]. Any recorded values outside of this range would be considered outliers and eliminated from further statistical analysis. It is generally suggested to calculate control limits at three standard deviations away from the mean; however, for the purpose of this

research it was decided that two standard deviations would induce a greater control on the process and reduce variability [28].

Table 3.1 – 2^3 full factorial experimental conditions for (a) wax, (b) ice

(a)

Trial	Infiltrant Hardness	Temp (°C)	Feed Rate (IPM)
1	Hard	-196	10
2	Very Hard	-196	10
3	Hard	-51	10
4	Very Hard	-51	10
5	Hard	-196	40
6	Very Hard	-196	40
7	Hard	-51	40
8	Very Hard	-51	40

(b)

Trial	Feed Rate (IPM)	Spindle Speed (RPM)	Corner Rad (In)
1	10	1000	0
2	40	1000	0
3	10	1200	0
4	40	1200	0
5	10	1000	0.02
6	40	1000	0.02
7	10	1200	0.02
8	40	1200	0.02

Two replications of this experiment were run for a total of 16 machining trials and then the results were analyzed in an Analysis of Variance (ANOVA) study. This ANOVA study will be discussed in greater detail later on in this chapter.

3.3.6 Analysis of Variance (ANOVA): ANOVA is used to study differences in the variances between groups and within the groups of a study. It was performed to study fitted main effects of the individual factors, two-factor interactions and combinations of pairs of factors, and interactions and combinations of all three factors. This exposed how infiltrant hardness, temperature, and feed rate interacted with each other to influence the resulting surface porosity of wax-infiltrated samples. It was also used to study the effect of feed rate, spindle speed,

and corner radius of the tool on ice-infiltrated samples. ANOVA helps to determine the significant effects of different arrangements of parameters, as well as the effect of each parameter alone. These software packages calculated all of the necessary values to determine which factors, or combination of factors, affected surface smearing based on the recorded surface porosity results. In addition, a one-way ANOVA was conducted to perform graphical analysis of fitted effects of the combination of different parameters. To analyze fitted effects, Indicator Function Parameterization was chosen over regular Effect Tests. The following sections provides details of the studies and results.

3.4 Results and Discussion:

The machining example illustrated in Figure 3.13 shows that there is an increase in pore occlusion when machining TM without infiltrant over time.

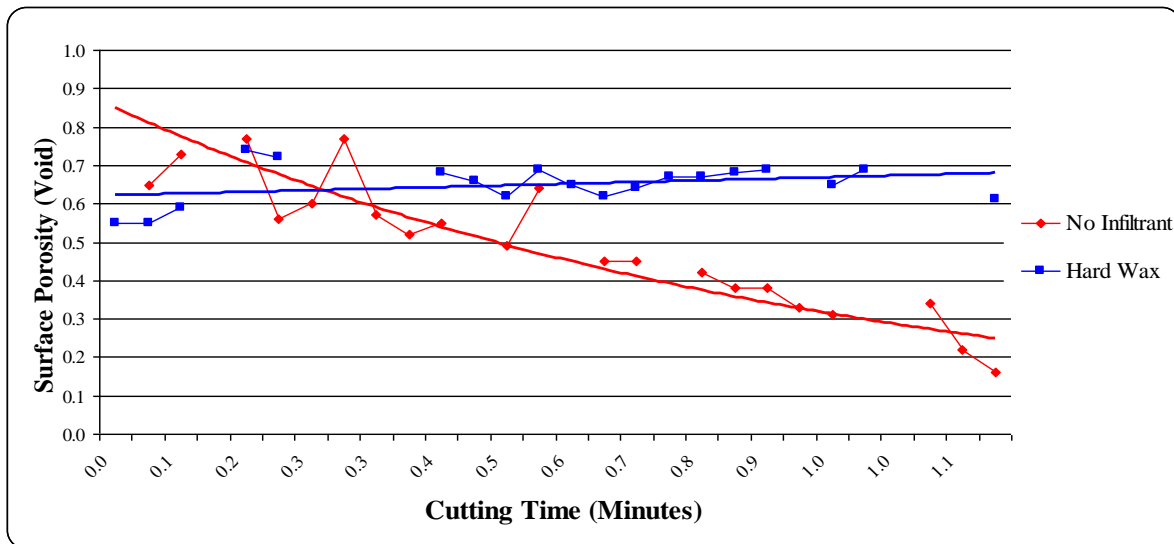


Figure 3.13 – The effect of surface smearing when using the infiltrant method [8].

It is also seen in this machining experiment that when using the infiltrant method, the surface porosity maintained an average value of approximately 65%. Unprocessed TM carries a nominal surface porosity measurement between 70 – 85% [10, 11, 12, 14]. In this example, the infiltrant method allowed machining to occur without significant pore occlusion; the surface porosity of the TM decreased about 10 – 15% over one minute of machining.

Table 3.2 lists different machining parameters for wax and ice-infiltrated samples with their associated values.

Table 3.2 – Investigated Machining Parameters for (a) wax and (b) ice-infiltrated samples

	(a)			(b)		
	Infiltrant Hardness	Temp. (°C)	Feed Rate (IPM)	Feed Rate (IPM)	Spindle Speed (RPM)	Corner Radius (in)
Low	Hard	-196	10	10	1000	0
High	Very Hard	-51	40	40	1200	0.02

A number of preliminary experiments were conducted resulting in approximately 300 individual surface porosity measurements. These experiments provided the base for selecting specific values for the two levels for final experimental trials.

Experiments Validation

In order to ensure that the results from trials conducted on wax sample are no different than results from the previous trials, an Upper and Lower 95% confidence interval was used. The results are shown in Table 3.3

Table 3.3 – Confidence Interval Test

Term	Estimate	Standard Error	DF Den	t Ratio	Prob> t	Lower 95%	Upper 95%
Intercept	0.80	0.015	5.00	53.95	<.0001*	0.760	0.840
A/B [A]	0.03	0.017	5.00	1.75	0.1411	-0.014	0.074
Feed Rate [10]	-0.10	0.017	5.00	-5.82	0.0021*	-0.144	-0.056

As shown in Table 3.3, the 95% confidence interval was calculated for factor A and B. Factor A refers to the series of data from trials conducted using wax while B was for ice. Lower and Upper confidence intervals for factors were found out to be -0.014 and 0.074 (Including 0). These values give evidence for the null hypothesis that there is no difference in the experimental results. However, detailed analysis with more data would be necessary to support the claim that there is no difference. This was not performed due to time constraints in this study.

Analysis of Wax-Infiltrated Samples

Table 3.4 – t-test results

2³ Full Factorial Analysis of Tools

In order to ensure that the results recorded from Tool A are different than those recorded from Tool B a *t*-test was conducted; this *t*-test assumed that the two data sets came from distributions with unequal variances. A mean surface

Mean
Variance
Observations
Hypothesized Mean Difference
df
t Stat
P(T<=t) one-tail
t Critical one-tail
P(T<=t) two-tail
t Critical two-tail

Tool A	Tool B
0.768	0.514
0.004	0.022
16	16
0	
21	
6.3	
0.000002	
1.721	
0.000003	
2.080	

porosity value was calculated for Tool A and Tool B that resulted in 0.77 and 0.51, respectively. The *t*-test results are shown in Table 3.4.

As shown in Table 3.4, the p -value ($P(T \leq t)$) resulted in 0.000003. This value is significantly lower than 0.05, so there is in fact a statistically significant difference in means between Tool A and Tool B. It is understood that p -values less than 0.05 are considered to be significant [29]. It was concluded that use of a new tool (Tool A) resulted in better surface porosity as compared to a used tool (Tool B).

ANOVA Results

For this research, three different experimental conditions were investigated through ANOVA analysis. A specific approach for analyzing a 3 Factor, 2 Level, and 8 Run DOE for variable data was used to perform analysis [29]. Since Tool A has favorable results, this analysis shows results of Tool A only.

Table 3.5 — All factorial results using Tool A

	Mean	A	B	C	AB	AC	BC	ABC
Sum +	6.145	3.130	3.120	3.290	3.055	3.035	3.075	3.050
Sum -	0.000	3.015	3.025	2.855	3.090	3.110	3.070	3.095
Overall	6.145	6.145	6.145	6.145	6.145	6.145	6.145	6.145
Difference	6.145	0.115	0.095	0.435	-0.035	-0.075	0.005	-0.045
Effect	0.768	0.029	0.024	0.109	-0.009	-0.019	0.001	-0.011
SS		0.003	0.002	0.047	0.000	0.001	0.000	0.001
MSE	0.042							

Factor A= Infiltrant Hardness, Factor B= Coolant Temperature, Factor C= Feed Rate

As shown in Table 3.6, feed rate (Factor C) was found to be a significant effect with an effect value of 0.109 ($Effect_C = 0.109 > MSE = 0.042$). This conclusion is

validated when looking at the ANOVA results that calculated p -value.

The p -value results for the experiment ran with Tool A are displayed in Table 3.6.

In reference to the p -value analysis, it was also concluded that infiltrant hardness and temperature (Factors A and B, respectively) may or may not have a significant effect on surface smearing.

Another way of analyzing the results from ANOVA is the use of ef-

fects charts. These visually depict the effect of the factor's interactions on the response. Fig-

ure 3.14 shows the individual main effects (infiltrant hardness, temperature, and feed rate) and the resulting average surface porosity values at their low and high parameter settings. The greater the change of magnitude in response values (demonstrated by the slope of a line, be it positive or negative) between the low and

high parameter setting, the more significant impact the factor interaction has on the response.

Table 3.6 – p -value results using Tool A

Factor	p -value
A	0.9075
B	0.8164
C	0.0000
AB	0.3653
AC	0.3653
BC	0.2235
ABC	0.4255

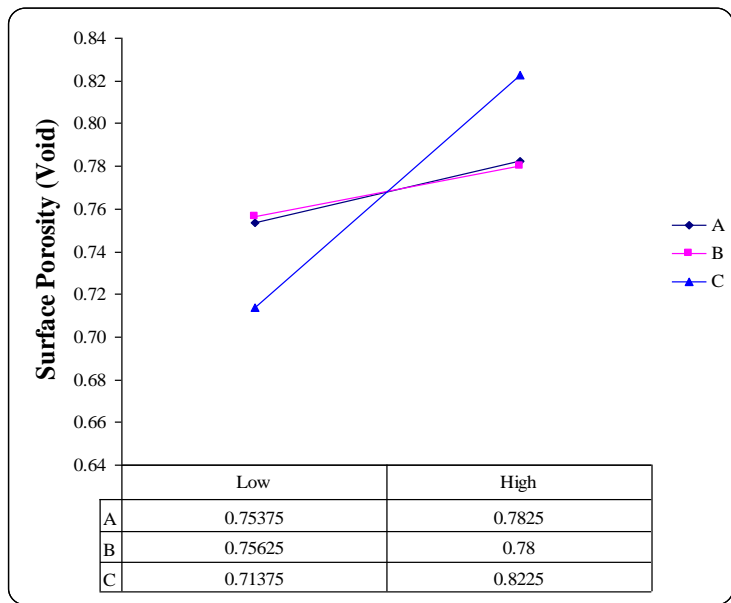


Figure 3.14 — Fitted main effect chart of Tool A

Analysis of Ice-Infiltrated Samples

ANOVA RESULTS

A model was created to study the effect of each factor on surface porosity individually and in combination.

$$\mu_y = \beta_1 X_1 + \beta_2 X_2 + \beta_3 X_3 + \beta_4 X_1 X_2 + \beta_5 X_1 X_3 + \beta_6 X_2 X_3 + \beta_7 X_1 X_2 X_3$$

Where X1= A= Feed Rate, X2= B= Spindle Speed, X3= C= Corner Radius of Tool. Table 3.7 provides the overall results of this analysis.

Table 3.7 — *Indicator Function Parameterization*

Term	Estimate	Standard Error	DF Den	t Ratio	Prob> t
Intercept	0.78835	0.014166	8.00	55.65	<.0001*
A[10]	-0.25335	0.020034	8.00	-12.65	<.0001*
B[1000]	-0.1067	0.020034	8.00	-5.33	0.0007*
C[0]	-0.05005	0.020034	8.00	-2.50	0.0370*
A[10]*B[1000]	0.0617	0.028332	8.00	2.18	0.0611
A[10]*C[0]	0.13	0.028332	8.00	4.59	0.0018*
B[1000]*C[0]	0.10505	0.028332	8.00	3.71	0.0060*
A[10]*B[1000]*C[0]	-0.11165	0.040067	8.00	-2.79	0.0237*

Factor A= Feed Rate, Factor B= Spindle Speed, Factor C= Corner Radius of Tool

By observing *p-values*, it was concluded that Factor A (Feed Rate) was the most significant factor. Considering the data in Table 3.7, it was concluded that Factor B and Factor C (Spindle Speed and Corner Radius) were also significant. In addition, the interaction of Factor A and C (Feed Rate and Corner Radius) was also found to be significant. However, the interaction of all three factors was not found to be as significant as individual factors.

One-Way ANOVA

Another way to analyze combination effects is One-way ANOVA. It was performed to study

the effect of combinations and to find optimal sets of combinations of factors. Figure 3.15 shows the relative surface porosity achieved by using different sets of combinations.

In these results: F = Feed Rate, S = Spindle Speed and C = Corner Radius of the tool. The number 1 or 2 indicates lower and upper level of

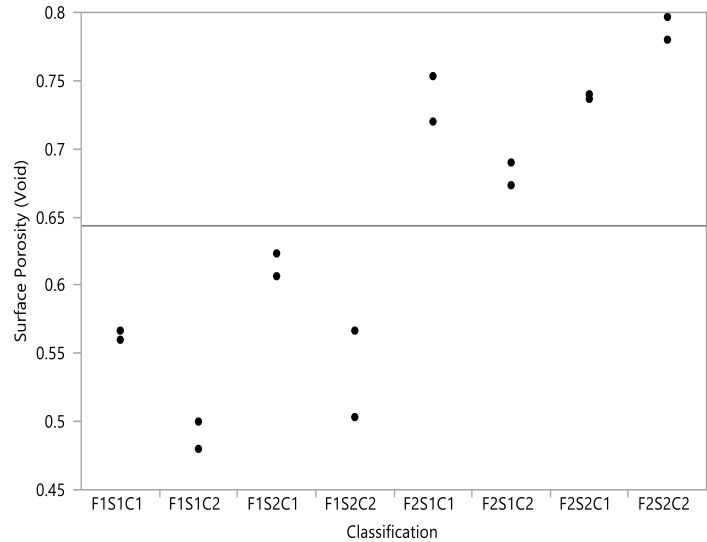


Figure 3.15 – One-way ANOVA for different combinations

the factors, respectively. It was concluded that the use of combination of F2S2C2 resulted in highest surface porosity; high speed, high federate, and large corner radius.

3.5 Implementation

As a result of the research explained in this thesis, utilizing the infiltration method presented reduces the effect of surface smearing while machining metal foam. In order to demonstrate process application for functional part geometries, the process was used to machine a bone fracture fragment from TM. The CAD model of the bone fragment was created from CT data taken from a human patient who sustained a high-impact leg fracture, Figure 3.16. The fracture was diagnosed as a comminuted tibial plafond fracture or the distal portion of the

tibia shattered upon impact, resulting in multiple segmental defects. The CT data of the patient's leg was used to excise geometric data for a large bone fragment to be machined. The bone fragment geometric data was extracted using Geomagic Studio® software to reverse engineer the segmental bone defects into individual sets of data points. The data points were then entered into Mastercam® where a 3-dimensional CAD file was created.

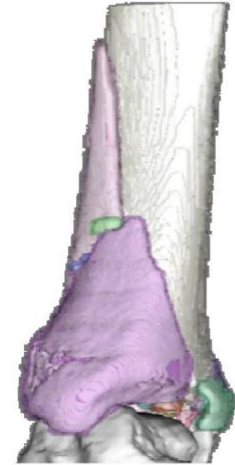


Figure 3.16 – *CT Scan Data*

The CNC-RP process used in this research begins after the sample has been infiltrated. The results of this analysis automatically determine all aspects of process planning for rapid machining the part, including tool path planning, tool geometry selection, machining setup orientations, and all necessary support fixturing geometry [30]. CNC-RP calculates the minimum number of machining orientations to create all necessary geometry, including any sacrificial support structures [30]. For example, a toy jack was machined using CNC-RP and it was determined that all surfaces could be machined from four cutting orientations. The cooling agents used in this research are a commercially available freezing spray, Cyto-Freeze™, and liquid nitrogen applied using a portable spraying unit. This rapid machining process example is illustrated in Figure 3.17 with the setup and processing steps taken to machine a toy jack. Much like traditional CNC milling, machining at specific feed rates and spindle speeds will affect the resulting surface finish. In this case, it is not so much important to maintain a certain aesthetic quality but rather to maintain the functionality of the cellular structure. The feeds, speeds, and machining temperatures evaluated in this research were chosen to maintain the solid state of the infiltrant during machining in

order to eliminate cell wall collapse. From the CAD model, CNC-RP software automatically analyzed the bone fracture fragment geometry and determined part orientation, sacrificial fix-
 ture support structures, cutting orientations, and cutting toolpaths before outputting the NC code [31].

The fracture fragment machined from TM was created from a 0.5-inch diameter bar stock. Due to the small diameter of the stock material, the same indexer used on the other prototypes could not be used. Instead, the bar was held within a collet that was secured to the machine table within a parallel jaw Chick™ vise. Due to the small diameter of the stock material, the geometric data of the fragment was scaled down in order to fit within

a 0.5-inch diameter. This scaling

operation was done within Mastercam® and then saved; to be analyzed with the CNC-RP software. Again, the CNC-RP software was run to determine all necessary cutting parameters. The parameters calculated for the TM sample were identical to those used before; however, the inability to use an indexer required the support structures to be modified. The three sacrificial supports created by CNC-RP were replaced with a single larger support centrally

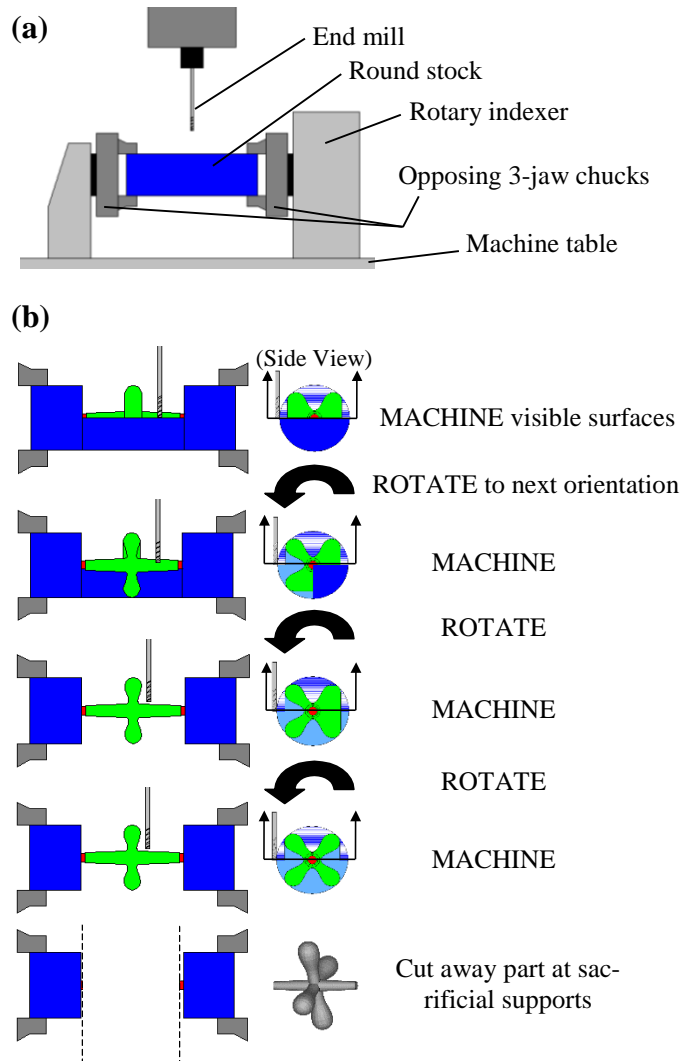


Figure 3.17 – CNC-RP rapid machining (a) set up and (b) processing steps for machining a toy jack [31].

placed along the x-axis. It was determined that all geometry could be machined from two orientations and instead of rotating the stock material in an indexer the collet was simply removed from the vise, rotated by 180 degrees, and then replaced.

The CAD representation with the sacrificial support and finished part are shown in Figure 3.18.

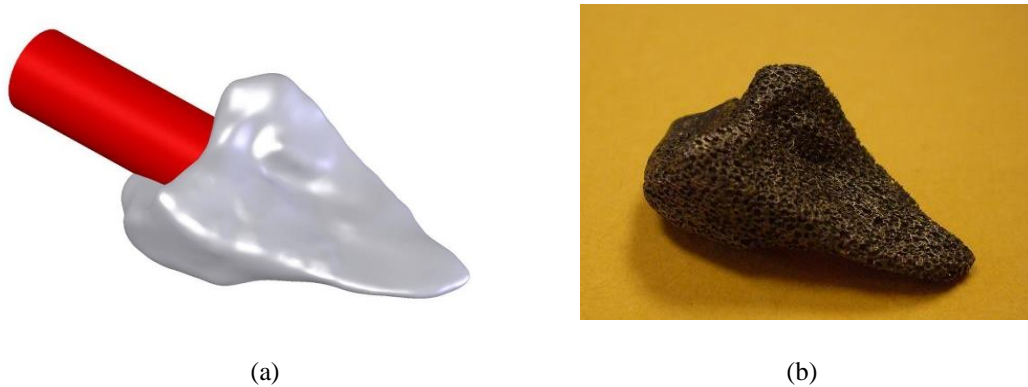


Figure 3.18 — *Sample bone implant, (a) CAD file with sacrificial support and (b) finished TM bone fracture fragment*

Before machining, the TM bar stock was infiltrated with very hard wax. During machining, the sample was continuously sprayed with Cyto-Freeze™ to keep the TM, wax, and tool cool. The fragment was cut with a 0.25 inch flat four flute HSS end mill. Upon machining completion, the bone fragment was cut from the remaining bar stock, the support was manually eliminated, and all residual infiltrant was removed. A reticle analysis was performed in the same manner as done in the 2³ full factorial analysis and a surface porosity of 69% was calculated from the measurements displayed in Table 3.8.

This is a successful example of the use of this new machining method; a custom bone fracture fragment was machined from patient-specific CT data, which, after post-processing, maintained a surface porosity value acceptable for Osseointegration in orthopedic surgery.

Table 3.8 — *Surface porosity analysis of TM bone fracture fragment*

Measurement	Surface Porosity (Void)	Average Surface Porosity (Void)
1	0.71	0.69
2	0.66	
3	0.70	

3.6 Conclusion

This study presents a novel machining method for metallic foams without surface smearing. The machining method presented in this work was subject to thorough experimentation in order to investigate the effects of certain machining parameters on the resulting surface porosity. Different machining parameters were investigated during this study. The influence of infiltrant hardness, machining temperature, machining feed rate, spindle speed, and corner radius of tool were studied. It was found that machining feed rate was most statistically significant effect, followed by spindle speed. Additional analysis indicated that tool wear and machining temperature also may influence surface porosity; however, these are subject to further investigation.

An ANOVA study conducted on wax-infiltrated samples proved that feed rate is the most statistically significant factor. It also suggested that temperature and infiltrant hardness may also be significant when machining with a newer tool. ANOVA performed on ice-infiltrated samples suggested that along with feed rate, spindle speed and corner radius of the tool were significant factors. A one-way ANOVA performed on ice-infiltrated samples indicated

that the combination of high speed, high feed and large corner radius reduces surface smearing. However, the combination of large corner radius with low feed and low speed increased surface smearing significantly. It was observed that some samples were distorted. It was believed that distortion might have caused because of increase in machining forces. However, detailed analysis is recommended to study the possible reason behind this issue.

Experimental results presented in this study suggest that the use of cooling agents does reduce the effect of surface smearing. Additional experimentation is recommended in order to discover which cooling agent works best in preserving the surface porosity value during machining. There seems to be a greater maintenance of surface porosity while milling when using liquid nitrogen when compared to Cyto-Freeze™, as well as when using Cyto-Freeze™ compared to no coolant at all.

Spindle speeds used for this study were selected based on preliminary test trials. All the wax trials were run at 1000 rpm. All the ice trials were run at either 1000 rpm and 1200 rpm. A future research endeavor should involve further exploration into what spindle speed should be used to minimize pore occlusion in different machining scenarios.

By combining this infiltration method with the CNC-RP technique, the machining of metallic foams without smeared surface is possible for custom geometric shapes. As demonstrated in the implementation section, custom bone fracture fragments were machined based on a patient's CT data. This study describes a new method to machine metallic foams along with maintaining their porosity. Implementation section provides an initial step toward the design and manufacture of custom orthopedic implants that could someday provide patients with more functionality and less discomfort due to a better fitting, stronger host bone attachment.

CHAPTER 4. CONCLUSION AND FUTURE WORK

Porosity is an important and essential characteristic of metallic foams. This thesis provides a new method to machine open cell metallic foams without compromising their surface porosity. Statistical data shows that ice as an infiltrant works as good as wax, with average surface porosity of all the trials conducted on ice infiltrated samples at 65%. Various machining parameters were investigated during this study, including machining feed rate, spindle speed, and corner radius of the tool. It was found that machining feed rate has the most significant effect, followed by spindle speed and corner radius.

By using the new infiltrant proposed in this thesis, it is now possible to machine metallic foams with greater efficiency. Ice as an infiltrant eliminated tedious post processing required in wax infiltration method. It was understood from a previous study that feed rate has a significant effect on the surface porosity of metallic foams when using wax infiltrant.

Experimental validation was performed on trials conducted using wax and trials conducted using ice. Lower and Upper 95% confidence interval for factors helped to understand any statistical difference in outputs of the trials, where it was found that there is no difference in the experimental results. An ANOVA study conducted on ice infiltrated samples provided valuable information about significant factors. In this work, the combination of feed rate and corner radius was also found to be significant. However, combinations of all 3 factors was not found to be as significant as individual factors. One-way ANOVA performed on ice infiltrated samples indicated that the combination of high speed, high feed and high corner radius reduces surface smearing significantly. However, the combination of high corner radius with low feed and low speed increased surface smearing significantly.

During machining trials of high corner radius tool, it was observed that some samples were distorted. It was believed that distortion might have caused because of increase in machining forces. However, detailed analysis is recommended to study the possible reason behind this issue. When observed through an optical microscope, tool flutes had metallic foam debris welded on them. It was believed that this might be caused because of high machining temperature. It also might be helpful to use coated tools instead of non-coated to avoid chatter, but further analysis is necessary to support this claim. It was found by fitted effects that higher spindle speed reduces surface smearing. However, contradictory to this, preliminary machining trials indicated that spindle speed higher than 1200 rpm resulted in higher surface smear. This might have occurred because ice began to melt due to elevated machining temperatures at higher speeds, however, further analysis is required to provide data to support this claim.

The work of this thesis provides a novel and effective method to machine metallic foams and could aid applications requiring porous, custom shaped metallic foams. In addition, it provides an improvement over wax infiltration due to reduced effort in post processing and the related risk of incomplete cleaning and contamination.

REFERENCES

- [1] A. Elements, "Metallic and Ceramic Foams," American Elements, 2016. [Online]. Available: <https://www.americanelements.com/foams.html>. [Accessed 24 02 2016].
- [2] M. F. Ashby, A. Evans, F. A. Norman, N. A. Fleck, L. J. Gibson, J. W. Hutchinson and H. N. Wadley, *Metal Foams - A Design Guide*, Boston: Butterworth-Heinemann, 2000.
- [3] G. Ryan, A. Pandit and D. P. Apatsidis, "Fabrication methods of porous metals for use in orthopaedic applications," *Biomaterials*, vol. 27, p. 2651–2670, 2006.
- [4] J. Black, "Biological Performance of Tantalum," *Elsevier*, pp. 167-173, 1994.
- [5] D. A. Shimko, V. F. Shimko, E. A. Sander, K. F. Dickson and E. A. Nauman, "Effect of Porosity on the Fluid Flow Characteristics and Mechanical Properties of Tantalum Scaffolds," *Journal of Biomedical Materials Research*, 2005.
- [6] V. Karageorgiou and D. Kaplan, "Porosity of 3D biomaterial scaffolds and osteogenesis," *Elsevier*, pp. 5474-5491, 2005.
- [7] M. D. T. D. M. S. V. M. G. a. J. F. Deglurkar, "Evaluation of Machining Methods for Trabecular Metal Implants in a Rabbit Intramedullary Osseointegration Model," *Journal of Biomedical Materials Research Part B: Applied Biomaterials*, vol. 80B:, pp. 528–540, 2007, 2006.
- [8] C. Hunt, "A method to reduce smearing in the milling of metal foams," Iowa State University, Ames, 2009.
- [9] M. P. Groover, *Fundamentals of Modern Manufacturing: Materials, Processes, and Systems*, Hoboken, NJ: John Wiley & Sons, Inc., 2010, pp. 637-640.
- [10] J. Banhart, "Manufacture, characterisation and application of cellular metals and metal foams," *Progress in Materials Science*, vol. 46, pp. 559-632, 2001.
- [11] L. J. Gibson and M. F. Ashby, *Cellular Solids: Structure and Properties- Second Edition*, New York: Cambridge University Press, 1999.
- [12] X. Wang, S. Xu, S. Zhou, W. Xu, M. Leary, P. Choong, M. Qian, M. Brandt and Y. M. Xie, "Topological design and additive manufacturing of porous metals for bone scaffolds and orthopaedic implants: A review," *Biomaterials*, vol. 83, pp. 127-141, 2016.
- [13] V. K. Balla, S. Banerjee, S. Bose and A. Bandyopadhyay, "Direct laser processing of a tantalum coating on titanium for bone replacement structures," *Acta Biomaterialia*, vol. 6, p. 2329–2334, 2010.
- [14] D. F. Williams, "On the mechanisms of biocompatibility," *Biomaterials*, vol. 29, no. 20, pp. 2941-2953, 2008.
- [15] J. D. Bobyn , G. J. Stackpool, S. A. Hacking , M. Tanzer and J. J. Krygier, "Characteristics of bone ingrowth and interface mechanics of a new porous tantalum biomaterial," *The Journal of Bone and Joint Surgery*, Vols. 81-B, pp. 907-914, 1999.

- [16] A. Werner , Z. Lechniak, K. Skalski and K. Kedzior, "Design and Manufacture of Anatomical Hip Joint Endoprostheses Using CAD/CAM Systems," *Materials Processing Technology*, vol. 107, pp. 181-186, 2000.
- [17] M. Truscott, D. d. Beer, G. Vicatos, K. Hosking, L. Barnard, G. Booyesen and I. R. Campbell, "Using RP to promote collaborative design of customised medical implants," *Rapid Prototyping Journal*, vol. 13, no. 2, pp. 107-114, 2007.
- [18] M. Bram, C. Kempmann, A. Laptev, D. I. Stöver and K. Weinert, "Investigations on the Machining of Sintered Titanium Foams Utilizing Face Milling and Peripheral Grinding," *ADVANCED ENGINEERING MATERIALS*, vol. 5, no. 6, pp. 441-447, 2003.
- [19] S. Chen, D. Head, M. Effgen and I. S. Jawahir, "An Investigation of Sustained Machining Performance for Controlled Surface Quality Requirements in Porous Tungsten," *IEEE TRANSACTIONS ON ELECTRON DEVICES*, vol. 52, no. 5, pp. 903-908, 2005.
- [20] O. R. Tutunea-Fatan, M. A. Fakhri and E. V. Bordatchev, "Porosity and cutting forces: from macroscale to microscale machining correlations," *Engineering Manufacture*, vol. 225, no. 5, pp. 619-630, 2011.
- [21] A. Salak, M. Selecka and H. Danninger, *MACHINABILITY OF POWDER METALLURGY STEELS*, Cambridge, UK: Cambridge International Science Publishing, 2005.
- [22] J. Schoop, I. S. Jawahir and T. J. Balk, "Size effects in finish machining of porous powdered metal foreengineered surface quality," *Precision Engineering*, vol. 44, p. 180-191, 2016.
- [23] W. O. Soboyejo and T. S. Shrivatsan, *Advanced Structural Materials: Properties, Design Optimization, and Applications*, Boca Raton, FL: CRC Press, Taylor & Francis Group , 2006.
- [24] W. D. Callister, *Materials science and engineering an introduction*, New York: Wiley, 1994.
- [25] M. Schwartz, *Brazing: For the Engineering Technologist (Manufacturing Processes and Materials Series)*, London: Chapman & Hall, 1994.
- [26] S. B. Vardeman and J. M. Jobe, *Statistical Quality Assurance Methods for Engineers*, New York, NY: Wiley & Sons, Inc. , 1999.
- [27] R. M. Warner, *Applied Statistics From Bivariate Through Multivariate Techniques*, Minneapolis, MI: Sage Publications, Inc., 2007.
- [28] T. A. Ratliff, *The Laboratory Quality Assurance System A Manual of Quality Procedures and Forms*, New York, NY: Wiley-Interscience, 2003.
- [29] S. Flashing, "A Basic Approach to Analyzing a 3 Factor 2 Level 8 Run DOE for Variable Data Video," YouTube, 2013.
- [30] M. C. Frank, R. A. Wysk and S. B. Joshi, "Rapid Planning for CNC Milling- A New Approach for Rapid Prototyping," *Journal of Manufacturing Systems*, vol. 23, no. 3, pp. 242-255, 2004.

- [31] M. C. Frank, R. A. Wysk and S. B. Joshi, "Using Subtractive Rapid Prototyping for Bone Replacement," in *Solid Freeform Fabrication Symposium*, Austin, 2008.
- [32] L. Brett, "A New Era in Porous Metals: Applications in Orthopaedics," *Advanced Engineering Materials*, vol. 10, no. 9, pp. 788-792, 2008.
- [33] G. J. Davies and S. Zhen, "Metallic foams: their production, properties, and applications.," *Journal of Materials Science*, vol. 18, p. 1899–1911, 1983.
- [34] C. Mas-Murano, B. Garrido, D. Rodriguez, E. Ruperez and J. Gil, "Biofunctionalization strategies on tantalum-based materials for osseointegrative applications," *Journal of Materials Science*, pp. 26-109, 2015.
- [35] G. Voort and F. Vander, *ASM Handbook Metallography and Microstructures* (ASM Handbook), New York: ASM International, 2004.
- [36] B. R. Levine, S. Sporer, R. A. Poggie, C. J. Della Valle and J. J. Jacobs, "Experimental and clinical performance of porous tantalum in orthopedic surgery," *Biomaterials*, vol. 27, p. 4671–4681, 2006.
- [37] J. J. Callaghan, A. G. Rosenberg and H. E. Rubash, *The Adult Hip*, Philadelphia: Wolters Kluwer, 2006.
- [38] A. Laptev, M. Bram, H. P. Buchkremer and D. Stover, "Study of production route for titanium parts combining very high porosity and complex shape," *Powder Metallurgy*, vol. 47, no. 1, pp. 85-92, 2004.
- [39] F. Matassi, A. Botti, L. Sirleo, C. Carulli and M. Innocenti, "Porous metal for orthopedics implants," *Clinical Cases in Mineral and Bone Metabolism*, vol. 10, no. 2, pp. 111-115, 2013.
- [40] I. Gibson, L. K. Cheung, S. P. Chow, W. L. Cheung, S. L. Beh, M. Savalani and S. H. Lee, "The use of rapid prototyping to assist medical applications," *Rapid Prototyping Journal*, vol. 12, no. 1, pp. 53-58, 2006.
- [41] J. Domanski, K. Skalski, R. Grygoruk and A. Mróz, "Rapid prototyping in the intervertebral implant design process," *Rapid Prototyping Journal*, vol. 21, no. 6, pp. 735-746, 2015.
- [42] M. C. Frank, "A method for machining metallic foam". United States of America Patent 61/024,945, 31 January 2008.
- [43] Zimmer, "Trabecular Metal Technology," Zimmer, 01 October 2012. [Online]. Available: http://www.zimmerdental.com/pdf/tm_materialbrochure2396.pdf. [Accessed 21 February 2016].
- [44] A. A. Dia, "Slideshare," Slideshare, 2013. [Online]. Available: <http://www.slideshare.net/aliaahmeddiaa/foam-by-alia>. [Accessed 15 02 2016].
- [45] Wikipedia, "Metal foams," Wikipedia, 2016. [Online]. Available: https://en.wikipedia.org/wiki/Metal_foam. [Accessed 2016].
- [46] D. . K. Pattanayak, A. Fukuda, T. Matsushita, M. Takemoto, S. Fujibayashi , K. Sasaki, . N. Nishida, T. Nakamura and T. Kokubo, "Bioactive Ti metal analogous to human cancellous bone: Fabrication by selective laser melting and chemical treatments," *Acta Biomaterialia*, vol. 7, p. 1398–1406, 2011.

- [47] A. L. Jardini, M. A. Larosa, C. A. d. C. Zavaglia, L. F. Bernardes, C. S. Lamberta, P. Kharmandayan, D. Calderoni and R. M. Filho, "Customised titanium implant fabricated in additive manufacturing for craniomaxillofacial surgery," *Virtual and Physical Prototyping*, vol. 9, no. 2, pp. 115-125, 2014.
- [48] I. Gibson, D. Rosen and B. Stucker, Additive manufacturing technologies 3D printing, rapid prototyping and direct digital manufacturing, New York: Springer, 2012.
- [49] M. C. Frank, S. Joshi and R. A. Wysk, "CNC-RP: A Technique for Using CNC Machining as a Rapid Prototyping Tool in Product/Process Development," in *Industrial Engineering Research Conference*, Orlando, FL, 2002.
- [50] S. L. Singare, L. Dichen, B. G. Zhenyu and L. Yaxiong, "Customized Design and Manufacturing of Chin Implant Based on Rapid Prototyping," *Rapid Prototyping Journal*, vol. 11, pp. 113-118, 2005.
- [51] S. Singare, L. Yaxiong, L. Dichen, L. Bingheng, H. Sanhu and L. Gang, "Fabrication of Customised Maxillo-Facial Prosthesis Using Computer-Aided Design and Rapid Prototyping Techniques," *Rapid Prototyping Journal*, vol. 12, pp. 206-213, 2006.
- [52] M. R. Meneghini, K. S. Ford, C. H. McCollough, S. D. Hansenn and D. G. Lewallen, "Bone Remodeling Around Porous Metal Cementless Acetabular Components," *The Journal of Arthroplasty*, vol. 25, no. 5, pp. 741-747, 2010.
- [53] Aponte, Javier, C. Cedeno, C. Ortiz, F. Samalot and G. Tiragallo, Biomechanics of Bone and Artery Replacement, 2003.
- [54] O. L. Harrysson, O. Cansizoglu, D. J. Marcellin-Little, D. R. Cormier and H. A. West II, "Direct Metal Fabrication of Titanium Implants with Tailored Materials and Mechanical Properties Using Electron Beam Melting Technology," *Materials Science and Engineering*, vol. 28, pp. 366-373, 2008.
- [55] R. Kaplan and Ultramet, "Open cell tantalum structures for cancellous bone implants and cell and tissue receptors". United States of America Patent 5,282,861, 1 February 1994.
- [56] R. Kaplan, H. Pierson, R. Tuffias, B. Williams and Ultramet, "High temperature resistant reticulated foam structure and process". United States of America Patent 5,154,970, 13 October 1992.
- [57] H. Ronal, Principles of Biomechanics, Boca Raton, FL: CRC Press, Taylor & Francis Group, 2008.
- [58] S. Patnaik, Strength of Materials- A unified theory, Amsterdam: Butterworth-Heinemann, 2004.
- [59] C. Shi, D. Head, M. Effgen and I. S. Jawahiri, "An Investigation of Sustained Machining Performance for Controlled Surface Quality Requirements in Porous Tungsten," *IEEE Transactions on Electron Devices*, vol. 52, pp. 903-908, 2005.
- [60] D. S. Adams, A Handbook of Measurements, Calculations, and Other Quantitative Skills for Use at the Bench, New York, NY: Cold Spring Harbor Laboratory Press, 2003.

APPENDIX A. 2³ FULL FACTORIAL EXPERIMENTAL RESULTS FOR WAX TRIALS

Factor A: Wax Hardness Factor B: Coolant Temperature Factor C: Feed Rate

Run	A	B	C
1	Hard	-51	10
2	Very Hard	-51	10
3	Hard	-196	10
4	Very Hard	-196	10
5	Hard	-51	40
6	Very Hard	-51	40
7	Hard	-196	40
8	Very Hard	-196	40
9	None	21	10
10	None	21	40

Tool A

Replicate	Run	Measurement			Average Surface Porosity (Void)	Control Analysis ($\pm 2\sigma$)	Cumulative Time (Minutes)
		1	2	3			
1	1	0.73	0.69	0.77	0.73	Not Outlier	1.39
	5	0.78	0.85	0.79	0.81	Not Outlier	1.40
	7	0.72	0.79	0.77	0.76	Not Outlier	1.41
	6	0.8	0.81	0.84	0.82	Not Outlier	1.42
	8	0.84	0.79	0.81	0.81	Not Outlier	1.43
	2	0.71	0.77	0.74	0.74	Not Outlier	1.50
	4	0.79	0.71	0.71	0.74	Not Outlier	1.55
	3	0.66	0.64	0.68	0.66	Not Outlier	1.59
	1	0.66	0.68	0.68	0.67	Not Outlier	1.63
	5	0.87	0.89	0.86	0.87	Not Outlier	1.64
2	7	0.85	0.84	0.81	0.83	Not Outlier	1.65
	6	0.84	0.83	0.84	0.84	Not Outlier	1.66
	8	0.83	0.85	0.85	0.84	Not Outlier	1.67
	2	0.74	0.74	0.79	0.76	Not Outlier	1.75
	4	0.7	0.69	0.74	0.71	Not Outlier	1.79
	3	0.72	0.7	0.69	0.70	Not Outlier	1.83

Tool B		Measurement			Avg	0.77	Std Dev	0.06
Replicate	Run	Average Surface Porosity (Void)			Control Analysis ($\pm 2\sigma$)	Cumulative Time (Minutes)		
		1	2	3				
1 and 2 (DOE created in SPC)	5	0.67	0.67	0.74	0.69	Not Outlier	4.95	
	1	0.3	0.39	0.44	0.38	Not Outlier	4.98	
	2	0.35	0.26	0.46	0.36	Not Outlier	5.02	
	7	0.65	0.67	0.63	0.65	Not Outlier	5.03	
	5	0.62	0.71	0.74	0.69	Not Outlier	5.04	
	2	0.39	0.3	0.46	0.38	Not Outlier	5.08	
	4	0.44	0.24	0.39	0.36	Not Outlier	5.12	
	1	0.17	0.39	0.39	0.32	Not Outlier	5.16	
	3	0.31	0.39	0.38	0.36	Not Outlier	5.20	
	4	0.52	0.42	0.42	0.45	Not Outlier	5.24	
	6	0.72	0.62	0.73	0.69	Not Outlier	5.24	
	8	0.65	0.6	0.68	0.64	Not Outlier	5.25	
	8	0.77	0.59	0.62	0.66	Not Outlier	5.26	
	3	0.42	0.37	0.42	0.40	Not Outlier	5.30	
	7	0.54	0.67	0.61	0.61	Not Outlier	5.31	
6	0.57	0.61	0.57	0.58	Not Outlier	5.32		
Avg					0.51			
Std Dev					0.15			

APPENDIX B. AVERAGE 2³ FULL FACTORIAL SURFACE POROSITY RESULTS PER FACTOR FOR WAX TRIALS

Tool A

	Low Setting	High Setting
	Avg. Surface Porosity (Void)	
Feed Rate	0.71	0.82
Infiltrant Hardness	0.76	0.78
Temperature	0.76	0.78

Tool B

	Low Setting	High Setting
	Avg. Surface Porosity (Void)	
Feed Rate	0.38	0.65
Infiltrant Hardness	0.51	0.52
Temperature	0.52	0.51

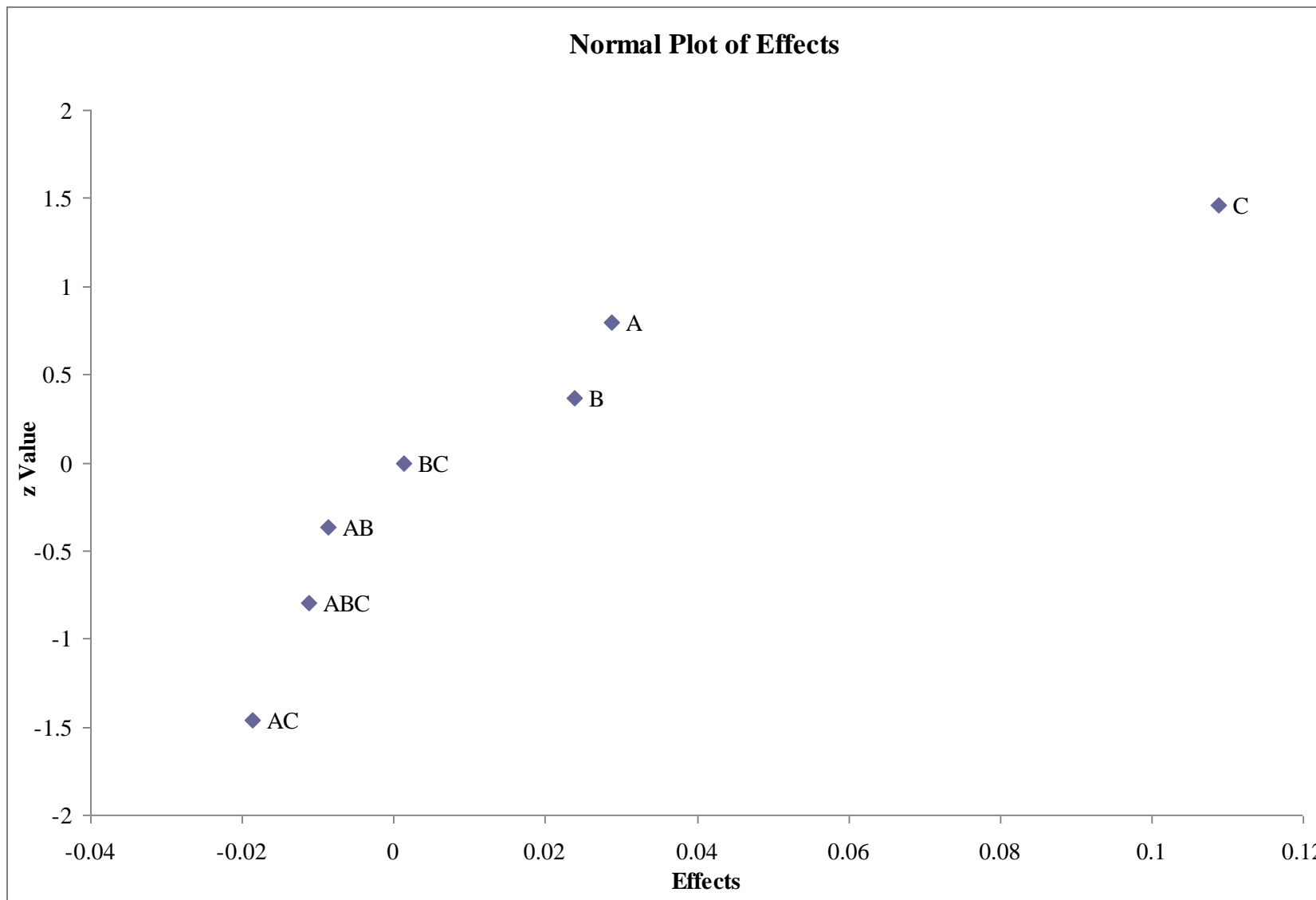
APPENDIX C. 2³ FULL FACTORIAL ANOVA ALL FACTOR ANALYSIS FOR WAX TRIALS - TOOL A

Design Table											
Standard Run Order	Mean	A	B	C	AB	AC	BC	ABC	Avg	Range	
1	+	-	-	-	+	+	+	-	0.68	0.04	
2	+	+	-	-	-	-	+	+	0.725	0.03	
3	+	-	+	-	-	+	-	+	0.7	0.06	
4	+	+	+	-	+	-	-	-	0.75	0.02	
5	+	-	-	+	+	-	-	+	0.795	0.07	
6	+	+	-	+	-	+	-	-	0.825	0.03	
7	+	-	+	+	-	-	+	-	0.84	0.06	
8	+	+	+	+	+	+	+	+	0.83	0.02	
Sum +	6.145	3.13	3.12	3.29	3.055	3.035	3.075	3.05			<i>The significant effects are in bold in the effects row. These are larger than MSE.</i>
Sum -	0	3.015	3.025	2.855	3.09	3.11	3.07	3.095			
Overall	6.145	6.145	6.145	6.145	6.145	6.145	6.145	6.145			
Difference	6.145	0.115	0.095	0.435	-0.035	-0.075	0.005	-0.045			
Effect	0.768	0.0288	0.0237	0.109	-0.00875	-0.0187	0.00125	-0.0113			
SS		0.00331	0.00226	0.0473	0.000306	0.00141	0.00000625	0.000506			
MSE	0.0422										

53

Range Chart Results		
Rbar	0.0413	<i>The ranges are in statistical control.</i>
UCLr	0.1348	
LCLr	None	

APPENDIX D. 2³ FULL FACTORIAL ANOVA NORMAL PLOT OF EFFECTS FOR WAX TRIALS - TOOL A



ANOVA Table Based on All Factors and Interactions						
Source	SS	DF	MS	F	p value	% Cont
A	0.0000250	1	0.0000250	0.014	0.9075	0.01%
B	0.000100	1	0.000100	0.058	0.8164	0.03%
C	0.303	1	0.303	174.101	0.0000	93.37%
AB	0.00160	1	0.00160	0.921	0.3653	0.49%
AC	0.00160	1	0.00160	0.921	0.3653	0.49%
BC	0.00303	1	0.00303	1.741	0.2235	0.93%
ABC	0.00122	1	0.00122	0.705	0.4255	0.38%
Error	0.0139	8	0.00174			4.29%
Total	0.324	15				100.00%

The significant factors are in dark shade ($p \leq 0.05$). Factors in light shade ($0.05 < p \leq 0.20$) may or may not be significant.

ANOVA for Model					
Source	SS	DF	MS	F	p value
Model	0.310	7	0.0443	25.494	0.0001

Average	0.51375
Standard Deviation	0.0417
Coefficient of Variation	8.114
R Square	95.71%
Adjusted R Square	91.96%
PRESS	0.0556
R Square Prediction	82.84%

Factor Information					
Factor	Coeff	DF	Standard Error	95% Lower	95% Upper
Intercept	0.514	1	0.010	0.490	0.538
A	0.00125	1	0.01042	-0.02278	0.02528
B	-0.00250	1	0.01042	-0.02653	0.02153
C	0.13750	1	0.01042	0.11347	0.16153
AB	-0.01000	1	0.01042	-0.03403	0.01403
AC	-0.01000	1	0.01042	-0.03403	0.01403
BC	0.01375	1	0.01042	-0.01028	0.03778
ABC	-0.00875	1	0.01042	-0.03278	0.01528

**APPENDIX E. 2³ FULL FACTORIAL DESIGN OF EXPERIMENTS FOR ICE
TRIALS**

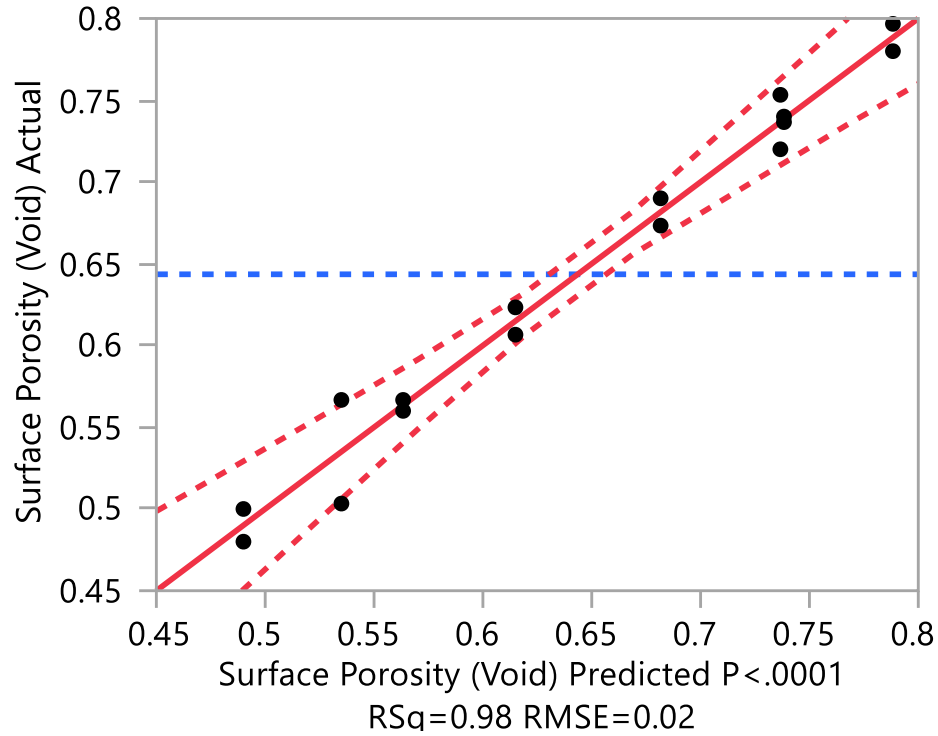
Factor A: Feed Rate, Factor B: Spindle Speed, Factor C: Corner Radius of Tool

Run	A	B	C
1	10	1000	0
2	40	1000	0
3	10	1200	0
4	40	1200	0
5	10	1000	0.02
6	40	1000	0.02
7	10	1200	0.02
8	40	1200	0.02

Replicate	Run	Measurement			Average Surface Porosity (Void)	Control Analysis ($\pm 2\sigma$)
		1	2	3		
1	3	10	1200	0	0.6066	Not Outlier
	4	40	1200	0	0.7366	Not Outlier
	1	10	1000	0	0.5667	Not Outlier
	2	40	1000	0	0.72	Not Outlier
	7	10	1200	0.02	0.5033	Not Outlier
	8	40	1200	0.02	0.7967	Not Outlier
	5	10	1000	0.02	0.48	Not Outlier
	6	40	1000	0.02	0.6733	Not Outlier
2	3	10	1200	0	0.6233	Not Outlier
	4	40	1200	0	0.74	Not Outlier
	1	10	1000	0	0.56	Not Outlier
	2	40	1000	0	0.75	Not Outlier
	7	10	1200	0.02	0.5667	Not Outlier
	8	40	1200	0.02	0.78	Not Outlier
	5	10	1000	0.02	0.5	Not Outlier
	6	40	1000	0.02	0.69	Not Outlier
				Avg	0.645	
				Std. Dev	0.106	

APPENDIX F. FITTED EFFECTS OF ICE TRIALS

Actual by Predicted Plot



Summary of Fit

RSquare	0.980952
RSquare Adj	0.964284
Root Mean Square Error	0.020034
Mean of Response	0.643531
Observations (or Sum Wgts)	16








Analysis of Variance

Source	DF	Sum of Squares	Mean Square	F Ratio
Model	7	0.16534905	0.023621	58.8549
Error	8	0.00321079	0.000401	Prob > F
C. Total	15	0.16855983		<.0001*

APPENDIX G. 2³ FULL FACTORIAL ANOVA ALL FACTOR ANALYSIS FOR ICE TRIALS

Source	Nparm	DF	Sum of Squares	F Ratio	Prob > F
Feed Rate	1	1	0.13751118	342.6232	<.0001*
Spindle Speed	1	1	0.01050113	26.1646	0.0009*
Corner Radius	1	1	0.00626077	15.5993	0.0042*
Feed Rate*Spindle Speed	1	1	0.00003452	0.0860	0.7768
Spindle Speed*Corner Radius	1	1	0.00242310	6.0374	0.0395*
Feed Rate*Corner Radius	1	1	0.00550193	13.7086	0.0060*
Feed Rate*Spindle Speed*Corner Radius	1	1	0.00311643	7.7649	0.0237*

Sorted Parameter Estimates

Term	Estimate	Std Error	t Ratio		Prob> t
Feed Rate[10]	-0.092706	0.005008	-18.51		<.0001*
Spindle Speed[1000]	-0.025619	0.005008	-5.12		0.0009*
Corner Radius[0]	0.0197813	0.005008	3.95		0.0042*
Feed Rate[10]*Corner Radius[0]	0.0185438	0.005008	3.70		0.0060*
Feed Rate[10]*Spindle Speed[1000]*Corner Radius[0]	-0.013956	0.005008	-2.79		0.0237*
Spindle Speed[1000]*Corner Radius[0]	0.0123062	0.005008	2.46		0.0395*
Feed Rate[10]*Spindle Speed[1000]	0.0014688	0.005008	0.29		0.7768

Indicator Function Parameterization

Term	Estimate	Std Error	DFDen	t Ratio	Prob> t
Intercept	0.78835	0.014166	8.00	55.65	<.0001*
Feed Rate[10]	-0.25335	0.020034	8.00	-12.65	<.0001*
Spindle Speed[1000]	-0.1067	0.020034	8.00	-5.33	0.0007*
Corner Radius[0]	-0.05005	0.020034	8.00	-2.50	0.0370*
Feed Rate[10]*Spindle Speed[1000]	0.0617	0.028332	8.00	2.18	0.0611
Spindle Speed[1000]*Corner Radius[0]	0.10505	0.028332	8.00	3.71	0.0060*
Feed Rate[10]*Corner Radius[0]	0.13	0.028332	8.00	4.59	0.0018*
Feed Rate[10]*Spindle Speed[1000]*Corner Radius[0]	-0.11165	0.040067	8.00	-2.79	0.0237*

**APPENDIX H. 2³ FULL FACTORIAL ANOVA INDIVIDUAL FACTOR ANALYSIS
FOR ICE TRIALS**

Effect Details

Feed Rate

Least Squares Means Table

Level	Least Sq Mean	Std Error	Mean
10	0.55082500	0.00708297	0.550825
40	0.73623750	0.00708297	0.736238

Spindle Speed

Least Squares Means Table

Level	Least Sq Mean	Std Error	Mean
1000	0.61791250	0.00708297	0.617913
1200	0.66915000	0.00708297	0.669150

Corner Radius

Least Squares Means Table

Level	Least Sq Mean	Std Error	Mean
0	0.66331250	0.00708297	0.663313
0.02	0.62375000	0.00708297	0.623750

Feed Rate*Spindle Speed

Least Squares Means Table

Level	Least Sq Mean	Std Error
10,1000	0.52667500	0.01001684
10,1200	0.57497500	0.01001684
40,1000	0.70915000	0.01001684
40,1200	0.76332500	0.01001684

Spindle Speed*Corner Radius**Least Squares Means Table**

Level	Least Sq Mean	Std Error
1000,0	0.65000000	0.01001684
1000,0.02	0.58582500	0.01001684
1200,0	0.67662500	0.01001684
1200,0.02	0.66167500	0.01001684

Feed Rate*Corner Radius**Least Squares Means Table**

Level	Least Sq Mean	Std Error
10,0	0.58915000	0.01001684
10,0.02	0.51250000	0.01001684
40,0	0.73747500	0.01001684
40,0.02	0.73500000	0.01001684

Feed Rate*Spindle Speed*Corner Radius**Least Squares Means Table**

Level	Least Sq Mean	Std Error
10,1000,0	0.56335000	0.01416595
10,1000,0.02	0.49000000	0.01416595
10,1200,0	0.61495000	0.01416595
10,1200,0.02	0.53500000	0.01416595
40,1000,0	0.73665000	0.01416595
40,1000,0.02	0.68165000	0.01416595
40,1200,0	0.73830000	0.01416595
40,1200,0.02	0.78835000	0.01416595

APPENDIX I. PREDICTION PROFILER

